THESIS FOR THE DEGREE OF DOCTOR OF PHILOSOPHY

Diffusion of large molecules in steam-exploded wood

Patric Kvist

Department of Chemistry and Chemical Engineering
CHALMERS UNIVERSITY OF TECHNOLOGY
Gothenburg, Sweden
2019

Diffusion of large molecules in steam-exploded wood

PATRIC KVIST
ISBN 978-91-7905-149-5

Doktorsavhandlingar vid Chalmers Tekniska Högskola
Ny serie nr 4616
ISSN 0346-718X

CHALMERS UNIVERSITY OF TECHNOLOGY
Department of Chemistry and Chemical Engineering
SE-412 96 Gothenburg
Sweden
Telephone + 46 (0)31-772 10 00

Printed by Chalmers Reproservice
CHALMERS UNIVERSITY OF TECHNOLOGY
Gothenburg, Sweden
2019

Diffusion of large molecules in steam-exploded wood

Patric Kvist

Department of Chemistry and Chemical Engineering
Chalmers University of Technology

Abstract

The diffusion of large molecules in wood pre-treated with steam explosion is important to understand in the context of the materials biorefinery. Steam explosion is a pretreatment method used to both open up the internal structure of wood and increase the accessibility of the cell walls of the wood with the use of high-pressure steam, and it is considered an energy-efficient method.

In this thesis, the diffusion of large molecules in wood pretreated with steam explosion is studied experimentally and through mathematical modeling. During steam explosion, wood biomass is subjected to saturated steam at elevated pressure and is followed by a quick release to atmospheric pressure. This treatment leads to mechanical ruptures and chemical modifications of the wood structure. Fluorescently marked dextran probes, up to 40 kDa in size, were used in combination with Fluorescent Recovery after Photobleaching to study diffusion in samples prepared with steam explosion. In this method, the fluorophore is bleached with a high intensity laser, the recovery of fluorescent intensity by the surrounding molecules is measured, and an effective diffusion coefficient can be calculated. Mathematical modeling was performed within the Lattice Boltzmann framework, utilizing images from a scanning electron microscope and high-resolution X-ray tomography, to reconstruct an accurate representation of the structural features of the microscale in wood.

The main findings of this thesis show that fluorescent diffusion probes can be utilized to investigate diffusion in both native wood and steam-exploded pretreated wood. A relative difference between earlywood and latewood is shown, and an increase in diffusion caused by the disintegration of the cell wall structure is found. The sub-micron features of the bordered pits, which enable radial transport between wood cells, were reconstructed, as well as the general microstructure in wood. The effective diffusion coefficient was computed by solving the diffusion equation for each structure. It was found that the outer borders covering the internal structure of the bordered pit totally dominate the mass transfer resistance. Transversal diffusion rates in the microstructure were found to increase after steam explosion, depending on the degree of disintegration and local volume investigated. The steam-exploded samples generally had a lower tortuosity, or shorter diffusion pathway, than native samples. Multiscale modeling was used to overcome the high computational demand of resolving the small features of a bordered pit at the microscale. The models presented used a variable diffusion coefficient where in the result for a single bordered pit is used.

Keywords: Wood, Diffusion, FRAP, Large Molecules, LBM, Steam Explosion

Acknowledgements

The research in this thesis was conducted within the Wallenberg Wood Science Center with financial support from the Knut and Alice Wallenberg Foundation, which is gratefully acknowledged. This project was also an associated project at SuMo Biomaterials, and their support is much appreciated.

I would also like to thank the following:

My main supervisor, Anders Rasmuson, for all the enjoyable meetings over the years.

Tobias Gebäck for everything simulation related.

My office mate Rasmus for various amusing discussions.

Adam Therning for his excellent work as a master's thesis student.

Anette Larsson for welcoming me into the SuMo family.

Niklas Lorén and Erich Schuster for experimental support and a great time in front of the microscope.

All my colleagues in WWSC, at SuMo, and at Chemical Engineering.

List of publications

I. Lattice Boltzmann simulations of diffusion through native and steam-exploded softwood bordered pits
Patric Kvist, Adam Therning, Tobias Gebäck, Anders Rasmuson (2017)
Wood Science and Technology, 51: 1261–1276.

II. Using fluorescent probes and FRAP to investigate macromolecule diffusion in steam-exploded wood
Patric Kvist, Erich Schuster, Niklas Lorén, Anders Rasmuson (2018)
Wood Science and Technology, 52: 1395–1410.

III. Lattice Boltzmann simulations of diffusion in steam-exploded wood
Patric Kvist, Tobias Gebäck, Mohammad Muzamal, Anders Rasmuson (2019)
Wood Science and Technology, 53: 855-871.

IV. A Multi-Scale Model for Diffusion of Large Molecules in Steam-Exploded Wood
Patric Kvist, Tobias Gebäck, Anders Rasmuson (2019)
Manuscript

Publication not included in this thesis

Analysis of mesoscale effects in high-shear granulation through a computational fluid dynamics–population balance coupled compartment model
Per Abrahamsson, Patric Kvist, Gavin Reynolds, Xi Yu, Ingela Niklasson Björn, Michael Hounslow, Anders Rasmuson (2017)
Particuology, 36: 1-12.

Contribution report

The author of this thesis has made the following contributions to the included papers:

I. Co-author. Performed experiments. Performed LBM simulations with second author. Interpreted results together with co-authors. Joint effort with second author in writing the paper.
II. Main author. Experiments were planned and performed together with second author. Interpreted results together with co-authors.
III. Main author. Performed modeling and simulations. Interpreted results together with co-authors.
IV. Main author. Performed modeling and simulations. Interpreted results together with co-authors.

List of abbreviations

CLSM – Confocal Laser Scanning Microscopy

FITC-dextran – Fluorescein isothiocyanate-dextran

FRAP – Fluorescent Recover after Photobleaching

ROI – Region of Interest

EW – Earlywood

LW – Latewood

SE – Steam explosion

SEW – Steam-exploded wood

SEIW – Steam-exploded and impacted wood

LBM – Lattice Boltzmann Method

SV – Sub-volume

Contents

1 Introduction

1.1 Background

A contemporary challenge facing society today is finding alternatives to the fossil-based industry that are both sustainable and renewable. Wood is a renewable resource available in vast quantities and has the highest density of energy among the biomass alternatives (Liu et al. 2012). Forest products have long been of great importance for the production of construction timber, cardboard, paper, and numerous hygiene products. However, the demand for printing paper has been declining with more and more digitalization of printing media. As incentives for sustainable materials increase, more and more research has focused on developing value-added products from wood. The available infrastructure and current knowhow of using wood as a feedstock make the forest industry a key factor in the transition to the biorefinery concept (Gomes et al. 2014).

The general definition of a biorefinery is a refinery that converts a renewable raw material to energy together with beneficial products. However, many different types of biorefineries exist, depending on which kind of platforms, products, feedstock, and processes are utilized (Cherubini et al. 2009). In the present work, the focus is on a materials biorefinery system with a base in the forest industry. In a materials biorefinery (Mattsson et al. 2017), it is desirable to obtain high molecular weight fractions of the main constituents of the wood cell wall: cellulose, hemicellulose, and lignin. However, to obtain large fractions of all three constituents, especially hemicellulose, from the highly recalcitrant wood cell wall in an efficient way is quite difficult. Often, a pretreatment step is employed to make the cell wall more accessible for enzymes, which can improve the yield of extraction of polymers by specific cleavage of covalent bonds (Azhar et al. 2011). However, the pretreatment must not be too harsh such that biopolymers are degraded during the process.

Several different methods to pretreat biomass exist today and include biological, chemical, physical, and thermal methods (Yang and Wyman 2012). The main goal of the pretreatment step is to induce some physical or chemical modification of the wood such that subsequent processing is improved. Steam Explosion (SE) is an extensively used physico-chemical pretreatment method for biomass (Alvira et al. 2010) that can also be used at milder conditions to open up the cellular structure of wood for easier processability (Agbor et al. 2011). At harsher conditions, i.e. higher pressures, a degradation of the main constituents, especially

hemicellulose, takes place to a greater degree (Wang et al. 2009). For a materials biorefinery, it is desirable to retain large molecular weight of the constituents, and thus, mild conditions are favorable.

A fundamental understanding of the mass transport of large molecules in and out of the wood material is crucial to understand the process of extracting valuable biopolymers. If both the extraction and separation of these can be achieved in an efficient way, the biopolymers can be used as raw materials for chemicals and value-added products. Large molecules include the native biopolymers present in native wood and enzymes that can be used to enhance the separation of cell wall components. The focus of the present research is on the diffusion of large molecules in wood pretreated with steam explosion. The inherent structure of wood has a major impact on mass transport in and out of the wood in the pretreatment step. This is also an important early step where hemicellulose can be extracted, which is an underused and large portion of the main wood constituents. Enzymes can be used in this stage to aid in the extraction of hemicellulose by accessing binding sites and cleaving specific covalent bonds (Azhar et al. 2011). The bulky enzyme macromolecule must diffuse through the microstructure in wood to reach these sites. Thus, it is important to understand both diffusion of wood biopolymers out of the structure and diffusion of enzymes into the material.

1.2 Objective

The main objective of the work in this thesis was to investigate the diffusion of large molecules in the context of the materials biorefinery. Specifically, the focus was on the upstream process of steam explosion. To this end, experimental work utilizing fluorescent probes and numerical simulations performed with the Lattice Boltzmann Method (LBM) were used.

1.3 Outline

Chapter 2 provides background information on wood and its cellular structure, and this is followed by the biorefinery concept, and steam explosion pretreatment. A general background to diffusion is presented along with the relevant literature on diffusion in wood. Experimental procedures are covered in Chapter 3, including equipment, materials, and methods used in this work. An introduction to the method of Fluorescent Recovery After Photobleaching (FRAP) is presented. Chapter 4 is dedicated to modeling. A general description of LBM is presented. This is followed by the geometries of the modelled microscale structures, which were based on both SEM and X-ray tomography images. The main results are summarized in Chapter 5 followed by concluding remarks in Chapter 6. The work in this thesis is based on the four papers appended at the end of the thesis.

1.4 Wallenberg Wood Science Center

The research presented in this work has been conducted within the Wallenberg Wood Science Center (WWSC). WWSC is a research center run jointly by the Royal Institute of Technology (KTH) and Chalmers University of Technology. It aims to build a material research program that can develop new material products and processes utilizing the Swedish forest. The research spans the whole chain from wood chips to value-added products. WWSC is based on a donation from the Knut and Alice Wallenberg Foundation.

2 Background

2.1 Wood

Wood is most commonly classified as either a softwood (conifers) or a hardwood (broad-leaf). Hardwoods are much more numerous, and the majority grow in tropical regions. The most relevant species in Sweden for industrial use includes the softwoods Norway spruce (*Picea abies*) and Scots pine (*Pinus sylvestris*). This study has focused on the softwood Norway spruce. Its unique structural features and chemical composition make for a very versatile material for many applications. Uses range from fuel and construction to furniture and tools to paper and packaging.

2.1.1 The structure and composition of softwood

Several different hierarchical levels of structure can be seen in softwood. The structure is usually divided into four sections in order of scale; macroscopic, microscopic, ultrastructure, and molecular structure.

Fig. 2.1 Yew wood (Taxus baccata) where the lighter part is sapwood and the darker part is heartwood. (Original source: Photo: MPF, November 2004, GNU Free Documentation License)

Cutting a tree stem transversely will reveal the general macroscopic structure of the wood, as seen in Fig. 2.1. The bark protects the inner part of the wood from both physical and biological degradation. The next layer of tissue on the inside of the bark is the phloem. The phloem is a living part of the wood responsible for transporting and storing nutrients. Following the phloem

is the vascular cambium, where the main growth of the stem occurs. The main part of the trunk is the xylem (secondary), the actual wood, which stretches from the cambium to the central pith. The pith is tissue formed during the first year of growth and is characterized by a circular dark spot in the center of the stem. The xylem is further divided into sapwood and heartwood; the former consisting of both living and dead cells, while the latter is only dead cells. The xylem is organized into annual growth rings. The rings are a consequence of the growth season and are divided into earlywood and latewood (Siau 1984; Sjöström 1993).

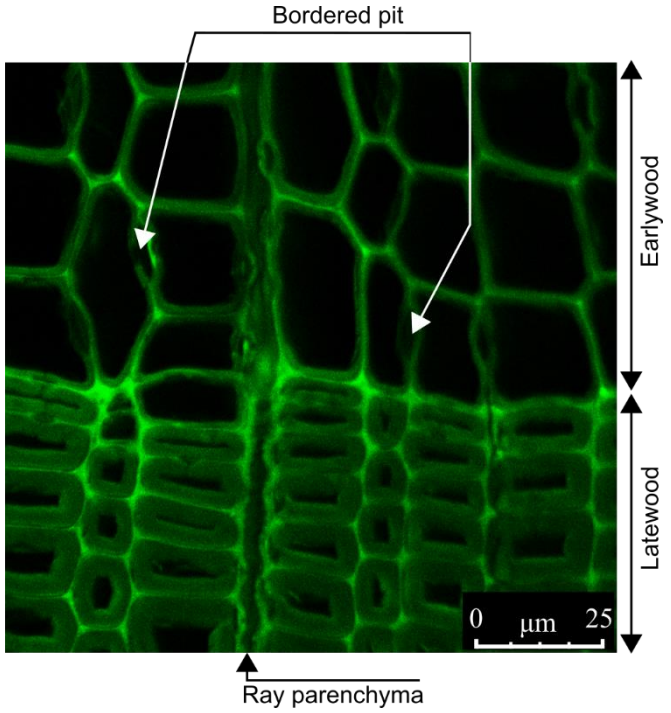

Fig. 2.2 CLSM micrograph of a water-impregnated cross-sectional slice of non-treated spruce for an excitation wavelength of 488 nm. The autofluorescent signal from lignin in the emission range of 500-650 nm illuminates the cell wall. The strongest signal is from the lignin-rich middle lamella. The green color was arbitrarly chosen to represent the signal, and a brighter shade indicates a stronger signal.

The softwood microstructure is comprised of mainly two cells: the tracheid and parenchyma. Almost all tracheids are in the longitudinal direction and have a length to diameter ratio of 100:1. Ray parenchyma, or ray cells, are in the radial direction towards the center of the wood. Tracheid cells make up 90-95 % of the xylem, while the other 5-10 % are ray cells (Brändström 2001). The general microscopic structure of a transversal cross-section of wood is shown in Fig. 2.2. A clear interface between the larger earlywood tracheids and the smaller latewood tracheids differentiate the figure in the middle. Among other things seen in the image are the bordered-pit pair that connect two tracheids together and enable transport between them. The detailed structure of a bordered pit is illustrated in Fig. 2.3 with the characteristic borders surrounding it with an impermeable torus in the center, which is suspended by the thin-stranded margo around it.

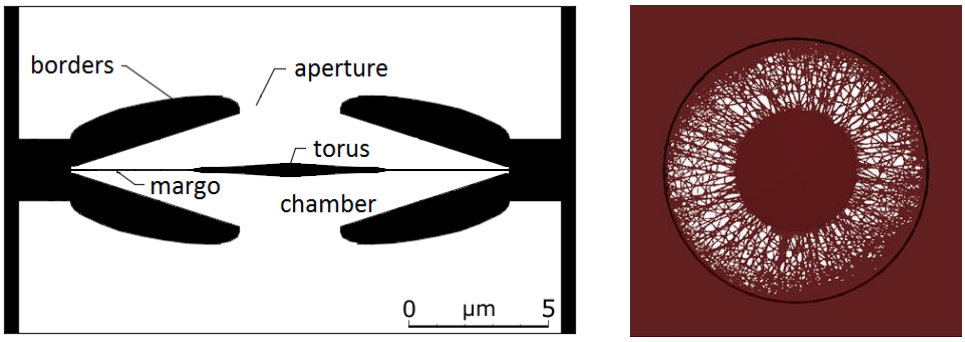

Fig. 2.3 General structure and nomenclature of a bordered pit can be seen to the left. The borders envelop the membrane-like structure of the margo and the impermeable torus in the center, seen to the right. The chamber is the open space within the bordered pit with the aperture leading into the pit.

The ultrastructure of the cell wall of a tracheid consists of multiple layers that differ significantly in size, in chemical composition, and in orientation. The three main layers are the S1, S2, and S3 layers, which comprise the bulk of the cell wall, while the middle lamella is located between the primary walls of two cells. The outer and inner layers of S1 and S3 are both very thin and difficult to analyze. Almost 80 % of the cell wall in Norway spruce consists of the S2 layer and is, due to this fact, much easier to characterize. There are multiple models that describe the arrangement of lignin, cellulose, and hemicellulose for the S2 layer, and the most commonly seen one is the model proposed by Kerr and Goring (1975).

Wood mainly consists of three components, cellulose, hemicellulose, and lignin. Cellulose is the most abundant component as it constitutes about 40-50 wt-% of wood. Hemicellulose and lignin make up about 20-30 wt-% each (Sjöström 1993). Cellulose is a polysaccharide composed of β-D-glucose units, which are connected by (1→4)-glycosidic bonds. The cellulose polymer is linear and tends to form intra- and intermolecular hydrogen bonds, and bundles of cellulose aggregate together to form microfibrils, which build up fibrils and finally cellulose fibers. Hemicelluloses are a group of heterogeneous polysaccharides. Unlike cellulose, hemicelluloses consist of shorter chains and can be composed of different sugar monomers and can vary between soft- and hardwoods. In softwood, the three main hemicelluloses are galactoglucomannan, glucomannan, and arabinoglucuronoxylan. Lastly, lignin is an irregularly structured polymer made up of aromatic phenylpropane units.

2.2 Biorefinery

The definition of a biorefinery is not always consistent, but the general framework is the use of a renewable raw material that produces value-added bio-products, such as chemical precursors, or bio-energy and bio-fuels, in a sustainable way (Gomes et al. 2014). Increasing societal awareness of environmental issues and legislation aid in the development of bio-based chemicals and energy (Liu et al. 2012). Fossil-based carbon is a finite resource, and replacing it with renewable carbon will be paramount to reduce emissions, which naturally leads to the development of biorefinery facilities (Cherubini et al. 2009).

Many different types of biorefineries exist and can be classified using the main features presented by Cherubini et al. (2009) in order of importance; platforms, products, feedstock, and processes. In this description, the biorefinery is defined by the pathway from feedstock to

products via platforms and processes. The focus of this work is specifically on the forest-based biorefinery. Wood is a very attractive feedstock compared to other biomass sources due to its large availability, high density, and that it does not compete with food (Liu et al. 2012). With the infrastructure of pulp mills in place and existing experience of handling wood as a feedstock make for an excellent platform for transition to future biorefineries.

In a materials biorefinery (Mattsson et al. 2017), it is desirable to obtain high molecular weight fractions of the three main constituents of the wood cell wall, namely cellulose, hemicellulose, and lignin, that are used as precursors for value-added bioproducts (Gomes et al. 2014). To separate these constituents from the recalcitrant cell wall, while retaining high molecular weight, requires mild process conditions in the upstream pretreatment steps to reduce hydrolysis and still facilitate accessibility. Cell wall separation may be further enhanced by the use of enzymatic hydrolysis of insoluble polysaccharides (Hasunuma et al. 2013). To increase the yield of an enzyme treatment, it is necessary to open the cell wall structure with the pretreatment of the wood (Azhar et al. 2011). Diffusion of large molecules in the porous microstructure of wood is important for understanding some of the limiting steps of an efficient materials biorefinery.

2.2.1 Pretreatment

The pretreatment of naturally recalcitrant wood is an important first step in the biorefinery process. There are various pretreatment methods available, all with different advantages and disadvantages (Agbor et al. 2011). It is unlikely that one method of choice for pretreatment will be optimal for all biomass, especially for different feedstocks (Agbor et al. 2011). However, milder conditions are preferable with respect to the materials biorefinery and utilization of all wood constituents. This allows for both the recovery of hemicellulose and increased accessibility of the cell wall. Examples of methods that allow for this are hot-water extraction and steam explosion. Neither method requires the use of a catalyst or additional chemicals. This work has specifically focused on steam explosion.

Steam explosion is the most common physico-chemical pretreatment method for wood (Alvira et al. 2010). In steam explosion, pressurized steam is introduced to wood chips for a short duration of time, after which the pressure is rapidly decreased to atmospheric conditions, allowing the steam to expand inside the wood, and a pressure gradient to develop between the wood and its surroundings. To keep degradation to a minimum while still achieving an increase in accessibility, the pressure of the steam is maintained at mild conditions, usually below 15 bars.

Steam explosion has been studied in regard to enzyme accessibility (Jedvert et al. 2012b; Muzamal et al. 2016) and structural effects both experimentally and by modeling (Muzamal et al. 2014, 2015). Wood porosity has also been shown to increase due to the expansion of water vapor in the wood cells during the release of high pressure to atmospheric pressure, which causes cracks in the cell wall and pits (Zhang and Cai 2006; Muzamal et al. 2015). These cracks increase the mass transport rates through the cellular structure.

2.3 Diffusion

Diffusion is a process of mass transfer caused by the random movement of molecules from a region of higher to lower concentration. Diffusion is a slow process, and, in many cases, it will limit the overall rate of transfer in a process. For example, diffusion limits the rate of industrial reactions that use a porous catalyst. It also controls the growth of microorganisms that produce penicillin and the rate of corrosion in steel (Cussler 2009). Similarly, diffusion limitations have also been shown to be relevant in wood processing (Hartler 1962; Siau 1984).

Fick developed the first mathematical description of diffusion (Fick 1855) using analogies from Fourier's work on conductive heat transfer. Fick defined the diffusional one-dimensional flux as:

$$J = -D\frac{\partial C}{\partial z} \tag{2.1}$$

where J is the rate of transfer per unit area, C is the concentration of the diffusing substance, z is the space coordinate, and D is the diffusion coefficient. For dilute systems, D can reasonably be taken as constant. The fundamental differential equation of diffusion is readily derived from Eq. (2.1) by considering a mass balance around an element of volume. It can then be shown that if the diffusion coefficient is assumed constant (Crank 1979), then:

$$\frac{\partial C}{\partial t} = D\nabla^2 C \tag{2.2}$$

This is sometimes referred to as Fick's second law of diffusion or the diffusion equation. It is analogous to the equation for heat conduction.

2.3.1 Diffusion coefficients in liquids

The most common way (Cussler 2009) to estimate the diffusion coefficient for large molecules in liquids is to use the Stokes-Einstein equation (Einstein 1905):

$$D_0 = \frac{k_B T}{f} = \frac{k_B T}{6\pi\mu R_0} \tag{2.3}$$

where f is the friction coefficient for the solute, k_B is the Boltzmann constant, μ is the solvent viscosity, and R_0 is the solute radius. The Stokes-Einstein equation is derived by assuming a rigid solute sphere that diffuses in a continuum of solvent, and this assumption generally seems correct for the diffusion of large spherical molecules and suspended particles in solvents of low molecular weight (Bird et al. 2007).

A polymer dissolved in a low molecular weight solvent is imagined as a long chain of segmented beads that form a random coil. The hydrodynamic size of the random coil will be different, depending on the type of solvent, temperature, and molecular weight. If the random coil is randomly distributed in an ideal solvent, the Stokes-Einstein equation can be used with an equivalent radius of the polymer as the root-mean-square radius of gyration (Cussler 2009):

$$R_e = 0.676\langle R^2\rangle^{1/2} \tag{2.4}$$

Light-scattering Rayleigh linewidth measurements have been performed by Sellen (1975) for dextran with molecular weights ranging from 10 to 500 kDa and the following correlation for diffusion coefficients for dextran was obtained based on molecular weight:

$$D_0 = 2.25 \times 10^{-4} M_w^{-0.45} \tag{2.5}$$

where D_0 is in mm^2/s, and M_w is in kg/mol. The correlation in Eq. (2.5) is in good agreement with conventional methods for molecular weights above 70 kDa, while for lower molecular weights the correlation is more uncertain due to polydispersity and possible presence of high molecular weight impurities (Sellen 1975).

2.3.2 Diffusion in porous media

A description of diffusion through liquid-filled pores of porous materials must consider the tortuous path through which the solute traverses the material along with the reduction in cross-sectional area. If the pores are not straight and the solid is impermeable to the solute, diffusion will take place over a longer distance than for a homogeneous material. To consider the deviation of a diffusion path from a straight line and the available cross-sectional area, the diffusion coefficient is scaled, or corrected, by tortuosity and porosity and is most commonly defined as an effective diffusion coefficient:

$$D_{eff} = \frac{\phi}{\tau^2} D_0 \tag{2.6}$$

where D_0 is the free diffusion coefficient of the species in the fluid present in the porous space, ϕ is the porosity, and τ is the tortuosity. Sometimes the "constrictivity" factor δ is used when the size of the diffusing species becomes comparable to the size of a pore (Boving and Grathwohl 2001). Different definitions of the effective diffusion coefficient based on porosity and tortuosity can be found in (Shen and Chen 2007).

Other diffusive mechanisms of transport in porous media include Knudsen diffusion (pore sizes comparable to the mean molecular free path) and surface diffusion of adsorbed molecules. These mechanisms are not included in the present work.

2.3.3 Diffusion in wood

Several studies regarding diffusion in wood have been conducted over the years. A general summary regarding moisture and drying can be found in the book by Siau (1984). The earliest study of dissolved molecules in wood is by Cady and Williams (1934) in which analogues to diffusion in gels are drawn to study the impact of the structure of solids on estimating effective mechanical blocking. Further, Burr and Stamm (1947) have derived theoretical models regarding transport of dissolved materials through softwoods for both the longitudinal and transversal directions based on a simplified model analogous to electrical conductance with resistance in series. The resistance in that study is estimated based on structural features, such as lumens, cell walls, and bordered pits.

Experiments have been conducted to estimate the effective diffusion coefficient of ions and organic molecules in wood with the use of diffusion cells (Cady and Williams 1934; Burr and

Stamm 1947; Christensen, G. 1951a, b; Behr et al. 1952; Narayanamurti and Kumar 1953). The impact of larger molecular compounds of polyethylene glycol (PEG) of various sizes up to 1.5 kDa on diffusion in native wood has been studied by (Fukuyama and Hiroyuki 1986) using a novel methodology with a refractometer (Fukuyama and Hiroyuki 1980) to measure concentration. The diffusion coefficient for the PEGs, in that study, was found to increase linearly with increasing molecular weight, up to 1.5 kDa.

The concentration profile for the diffusion of ions has been studied in a number of different experimental and modeling set-ups. A staining technique was used by Jacobson et al. (2006) to study the diffusion of sulfide and hydroxide simultaneously. Model predictions for the impregnation of NaOH before steam explosion treatments were created by (Kazi et al. 1996). The model used experimental data obtained from SEM X-ray intensity measurements. Diffusion experiments with LiCl have been performed by Kolavali and Theliander (2013) based on the low affinity of Li toward native wood components and on the low natural content of the ion in wood. The samples in that study, were immersed in solution for different amounts of time after which the samples were cut from different locations and analyzed with atomic emission spectroscopy. Subsequently, concentration profiles of Li were obtained as a function of dimensions, impregnation time, structure, and temperature.

Model systems that mimic a wood cell wall in the form of gels have been investigated using fluorescent probes in order to study the influence of the size of the diffusion probe and the influence of a porous gel mesh size (Paës and Chabbert 2012). The hydrodynamic radius of the dextran diffusion probe was found to influence diffusion more than the porous size of the mesh. For a protein probe, indications of anomalous diffusion have been observed and have been attributed to interaction with the gel. Similarly, studies on the size dependency of molecules have been conducted by Yang et al. (2013) in which dextran is used as a diffusion probe in a porous structure. The structure was made from milled filter paper to evaluate the influence of pore size distribution on diffusion.

Further studies on gel structures have been conducted using FRAP to assess the effect of substrate hydrolysis and substrate binding on the mobility of wood-related enzymes (Cuyvers et al. 2011). A more rigorous study on the mechanisms of carbohydrate binding modules (CBMs) has been carried out by Paës et al. (2015) utilizing FRAP and a set of similar CMBs in a variation of bioinspired assemblies to assess enzymes relevant for biorefining. FRAP has also been used to investigate diffusion in the wood cell wall of several different types of chemically pretreated samples to investigate the impact of the pretreatment method, the size of the diffusion probe, and cell wall localization (Paës et al. 2017).

Diffusion through bordered pits has been estimated by (Petty 1973) based on the old models by (Stamm 1946) with new data for the structure and permeability of wood. The resistance due to structural features was estimated based on the model, and it was found that the resistance to diffusion was as high as 15 % for the pit membrane, while the remaining resistance was attributed to the borders. Further numerical modeling was performed on a single bordered pit by Wadsö (1988) with a finite difference method, and the conclusion was that the resistance of the margo and torus should be minor compared to the resistance of the borders.

Even though diffusion has been studied on the cellular level in wood, nevertheless, a detailed high-resolution study is lacking, in particular, one with relevance for larger molecules, such as high molecular weight polysaccharides and enzymes. Of special interest is to study the effect of steam explosion, in which the increased accessibility and opening of the cellular structure in wood is key to both the impregnation of samples with enzymes and the extraction of biopolymers.

3 Experimental

Chapter 3 covers the experimental procedures, sample preparation, and equipment used. The general principle of the FRAP method is covered along with the model used to evaluate the data obtained.

3.1 Fluorescent Recovery after Photobleaching

FRAP was first developed as a technique to measure the transport of proteins and lipids in living cells (Axelrod et al. 1976), and it has been further generalized and developed by Kang et al. (2009). This technique has since then been used to study the transport of various different proteins in a number of cell membranes and living cells (Lorén et al. 2015). Apart from the field of cell biology, FRAP has found an important foothold in pharmaceutical research due to the technique's non-invasiveness and high specificity, which make it useful in measuring diffusion in vivo in complex materials (Deschout et al. 2014). Hydrogels have been especially interesting for a time-controlled drug delivery system in which the heterogeneous structure inside the gel controls the delivery. Several studies have been conducted with FRAP to characterize the diffusive process in different gel structures (Videcoq et al. 2013; Schuster et al. 2014, 2016; Lopez-Sanchez et al. 2015; Peixoto et al. 2015). FRAP has also been successfully used in food technology in which the microstructure of food often is a multiphase mixture of, e.g. gels, foams, and emulsions (Wassén et al. 2014) where mass transport mechanisms control the final properties of the food product.

Utilizing a confocal microscope to direct a high intensity light into a region of interest (ROI), fluorescent molecules can be irreversibly bleached. This imposes a concentration gradient on the bleached area, causing bleached molecules to diffuse out and unbleached molecules to diffuse into said area. The recovery of intensity in this area is a function of how fast unbleached molecules diffuse into the area. Dextran labeled with the fluorophore isothiocyanate (FITC) is commonly used as a diffusion probe in FRAP experiments (Deschout et al. 2014).

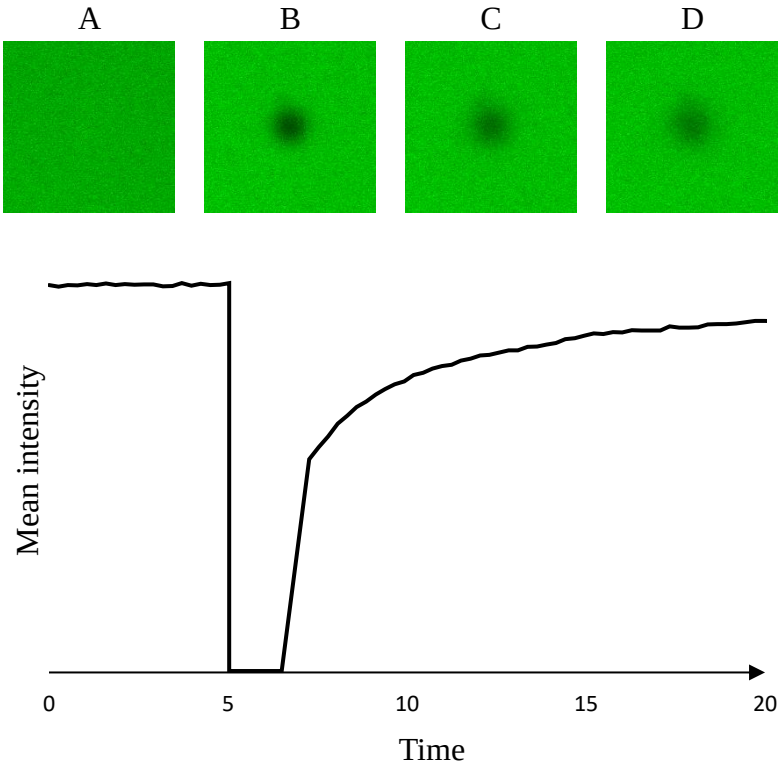

Fig. 3.1 FRAP recovery curve of the mean intensity over time. Measurement was done on a Dextran-FITC diffusion probe in aqueous solution.

The principle of FRAP is best illustrated with a simple figure that shows the entire bleaching process. In Fig. 3.1, the initial part (A) corresponds to the pre-bleach period where the intensity is measured to confirm that no non-intentional bleaching has been done by the background laser, thus, it is desirable to have a flat profile during this period. The pre-bleach period is followed by a high intensity laser pulse for a few frames, which is followed by a subsequent measurement of the intensity recovery (B, C, and D) over time. The amount of bleaching is a compromise between not damaging the sample, due to high photon flux, and achieving good recovery data that can be analyzed (Lorén et al. 2015).

The data from the recovery is analyzed using a diffusion model that relates the recovered intensity to a diffusion coefficient. The simplest models are empirical models that consider the shape of the recovery curve through a simple exponential function (Kapitza et al. 1985). While these models are easy to use and can be used in a comparative study, it has no general theoretical basis and rarely yields accurate values. More reliable models for obtaining quantitative information are closed form models that rely on a theoretical description of the entire diffusional FRAP process. Many different closed form models exist, reviewed in, e.g. Lorén et al. (2015).

3.1.1 Confocal Scanning Laser Microscopy

Both imaging and diffusion experiments were performed with a Leica SP5 confocal microscope AOBS (Heidelberg, Germany). All wood samples analyzed were prepared by slicing 200-300 μm thick sections with a high-profile disposable blade. Each slice was mounted on a cover glass in which a small well was created by layering spacers to hold the sample and solution in place. The laser wavelength used was 488 nm.

3.1.2 FRAP protocol

The FRAP measurements were carried out at room temperature (22 C°) with the following settings: image format 256 × 256 pixels; zoom factor 4 (with a zoom-in during bleaching); and scanning rate 1000 Hz, rendering an image acquisition rate of 0.265 s per image and a pixel size of 0.73 µm. The FRAP images were stored as 12-bit tiff-images. The images were recorded using a PMT detector. The FRAP protocol consisted of 20 pre-bleached images, and 1 - 4 bleached images depending on the probe, followed by 50 images during the recovery process. Five measurements were performed per region investigated. In this work, bleaching refers to the stage where a higher laser intensity is applied to photobleach some of the fluorescent molecules in the region of interest.

The fluorescent diffusion probes Fluorescein isothiocyanate–dextran (FITC-dextran) 3 kDa, 10 kDa and 40kDa (Invitrogen Molecular Probes, Eugene, OR) were dispersed in deionized water to yield 150 ppm. Polypropylene beakers were sealed with tin-foil to protect them from light source degradation and were stored in a refrigerator prior to use.

3.1.3 FRAP model

A model developed by Jonasson et al. (2008), which is a pixel-based framework for analyzing FRAP data, was used. The model assumes that a circular area is bleached and that the initial fluorophore concentration profile can be approximated by a Gaussian function:

$$C_0(r) = a_0 - \frac{a_1}{r_0^2} exp\left(-\frac{r^2}{r_0^2}\right) \tag{3.1}$$

where a_0, a_1, and r_0 are constants, and r is the distance from the center of the bleached area. The constants can be obtained by fitting the first bleached image pixel values. The recovery process continues in time as described by a Gaussian distribution, which is a Gaussian function according to:

$$C(r,t) = a_0 - \frac{a_1}{4Dt + r_0^2} exp\left(-\frac{r^2}{4Dt + r_0^2}\right) \tag{3.2}$$

The diffusion coefficient is later found by fitting the recovery image pixel values using the maximum-likelihood method.

3.2 The Steam Explosion process

A general depiction of the SE equipment built at Chalmers is shown in Fig. 3.2. The experiments were performed at a pressure of 14 bar for 10 minutes after which the pressure was released to atmospheric conditions. As the pressure is released, the samples discharge into the so-called blow tank and were collected at the bottom of the equipment. As the discharge occurs, the wood samples gain high velocities and collide with each other and, especially, with the walls of the blow tank. Depending on velocity and impact angle, the wood samples can disintegrate into smaller fragments. To separate the explosion step from the impact step in the present research, several samples were secured in a basket that prevented them from being forced down into the

lower chamber. Being fixated in the upper larger steam tank also meant that the samples were exposed to high temperatures for a longer time because the equipment needed time to cool before it was possible to remove the samples.

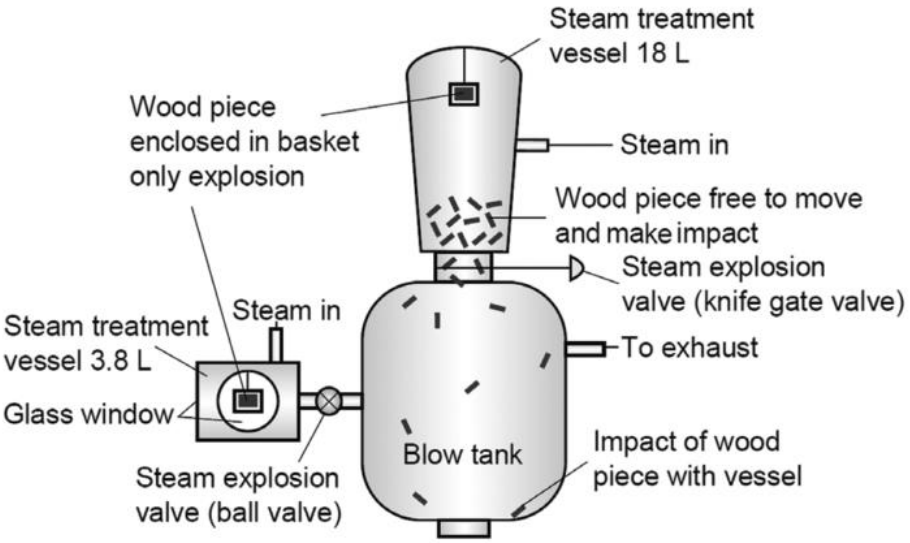

Fig. 3.2 General schematic description of the steam explosion equipment at Chalmers (Muzamal et al. 2015).

3.3 High-resolution X-ray tomography

High-resolution X-ray tomography was performed at the Ångström Laboratory of Uppsala University (Uppsala, Sweden). The projections obtained from the X-ray scan were reconstructed into stacks of 2D 16-bit BMP images using the software nRecon 1.6.10.1 (Bruker, Sweden). The stacks contained up to 1700 images of cross-sections perpendicular to the longitudinal tracheids. The native and SE-1 samples had an isotropic voxel size of 0.81 μm. The SE-2 sample had a slightly higher resolution and an isotropic voxel size of 0.54 μm. The images were cropped and converted into 3D TIFF stacks of 200 images, where each image slice represented a thickness of 0.81 and 0.54 μm.

3.4 Wood samples

All samples were prepared from a stem of Norway spruce (*Picea abies L.*) disc, cut into 4x20x130 mm rectangles, and stored in airtight polyethylene bags in a freezer. Before further use of the samples, the wood pieces were defrosted for at least 24 hours. Samples were then cut into smaller 4x20x20 mm pieces before the steam explosion treatment. The naming convention for the samples differ for Paper II and Paper III, as seen in Table 3.1.

Table 3.1 Collection of the prepared samples used in the experimental part of the thesis.

FRAP measurements (Paper II)		X-ray tomography (Paper III)	
Sample	**Label**	**Sample**	**Label**
Native wood	Native	Native wood	Native
Steam-exploded wood	SEW	Steam-exploded and impacted wood	SE-1
Steam-exploded and impacted wood	SEIW	Steam-exploded and impacted wood	SE-2

3.4.1 Preparation of samples for FRAP (Paper II)

Three different wood samples were prepared to analyze both the physical and chemical effects of steam explosion: Untreated native wood as the reference, steam exploded wood (SEW), and steam exploded and impacted wood (SEIW). Both steam-exploded samples showed sign of discoloration due to the high temperature of the steam explosion pretreatment, as seen in Fig. 3.3.

A total of 16 samples were used in the steam explosion equipment. Six of the samples were secured with a fixture to separate them from the impact step, while the rest were loaded as normal in the steam tank. Steam-exploded wood was obtained after introducing saturated steam at 14 bars (198 °C) in the steam tank for a total of 10 minutes. The pressure was quickly released to atmospheric conditions, and the non-fixated samples rapidly escaped into the flash tank and were collected along with condensed steam. The steam-exploded and native samples are shown in Fig. 3.3.

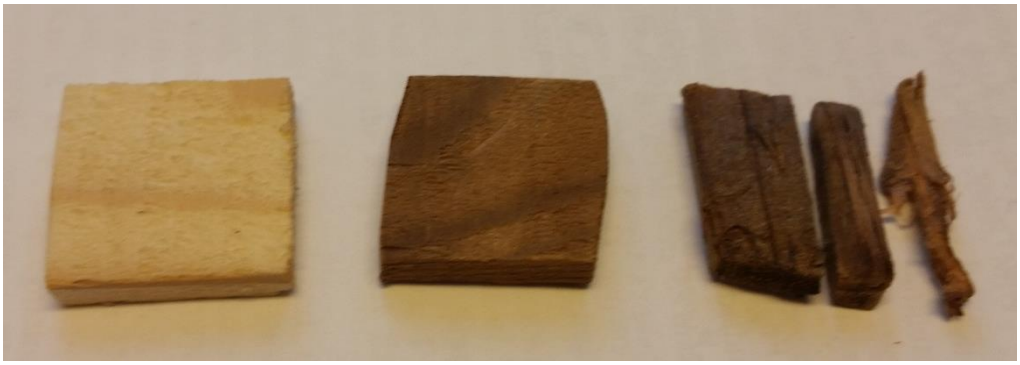

Fig. 3.3 From left to right: Native, SEW, and SEIW. Notice the color change after treatment present in both samples subjected to steam explosion. The SEIW samples show distinct ruptures mostly in the fiber direction.

3.4.2 Preparation of samples for tomography (Paper III)

Wood samples and the preparation of samples for high-resolution X-ray tomography were performed by Muzamal et al. (2016). The subsequent images obtained using X-ray tomography were used in this work. The sample preparation was the same as described in Section 3.4.1. The main difference was that only impacted steam-exploded wood was used. This was due to the expected similarity of the microstructure in a comparison of native and non-impacted steam-exploded wood. The steam treatment by itself caused minor physical modifications due to the

degradation of hemicellulose (Muzamal et al. 2015) and some shrinking due to thermal treatment (Van den Bulcke et al. 2013).

The pretreatment created large structural changes in different-sized fragments, some completely defibrillated while others remained relatively intact. To investigate the differences between these fragments two samples were selected for X-ray tomography. Sample SE-1 was chosen because it had relatively little damage compared to sample SE-2, which sustained major damage. These samples were further cut into small cubes, approximately 1.4 mm, to obtain X-ray scans at a high resolution. The same procedure was done with the native reference sample. Mainly earlywood was sampled because of the larger size of both the lumina and bordered pits of earlywood compared to latewood.

4 Modeling

The modeling is divided into two parts. The first part covers the modeling of a bordered pit based on SEM images. The second part covers the modeling of the microstructure in wood based on X-ray tomography. All simulations were performed using the Lattice Boltzmann Method (LBM).

4.1 Lattice Boltzmann Method

LBM has shown great promise for simulations in complex geometries due to its cost-efficient implementation of boundary conditions and ease of parallelization (Zhou 2004; Bernsdorf 2008; Gebäck et al. 2015).

For a system without an external force, the Boltzmann transport equation can be written as:

$$\frac{\partial f}{\partial t} + \boldsymbol{c}\nabla f = \Omega \tag{4.1}$$

where f is a distribution function of time, space, and velocity. $\boldsymbol{c}$ is the velocity vector, and Ω is the collision operator. The collision operator is a function of f and must be determined to solve the Boltzmann equation.

One complication of solving the Boltzmann equation is the complexity of the collision term. Bhatnagar, Gross, and Krook (BGK) (Bhatnagar et al. 1954) have introduced a simplified model to replace the collision operator:

$$\Omega = \omega(f^{eq} - f) = \frac{1}{\tau_r}(f^{eq} - f) \tag{4.2}$$

where $\omega = {}^{1}/_{\tau_r}$. The coefficient ω is the collision frequency, and τ_r is called the relaxation factor. A local equilibrium distribution function f^{eq} is introduced, which is a Maxwell-Boltzmann distribution function. With the BGK simplification introduced, the Boltzmann equation can be written:

$$\frac{\partial f_i}{\partial t} + \boldsymbol{c_i}\nabla f_i = \frac{1}{\tau_r}\left(f_i^{eq} - f_i\right) \tag{4.3}$$

where *i* denotes the streaming direction of the computational lattice grid. The above equation can be discretized as:

$$f_i(x + c_i\Delta t, t + \Delta t) = f_i(x, t) + \frac{\Delta t}{\tau_r}\left[f_i^{eq}(x, t) - f_i(x, t)\right] \tag{4.4}$$

All parameters are dimensionless, and the domain is discretized into an equal-sized lattice grid. Particles are allowed to occupy points on both the surface and in the interior of the lattice. The arrangement of the lattice domain is often represented with the setup D_nQ_m, where n denotes dimension (1D, 2D, and 3D), while m denotes the number of linkages. For 3D simulations, one of the more common setups is the D3Q19, which is visualized in Fig. 4.1. In essence, more linkages would translate into higher resolution, however, this would lead to higher computational demand.

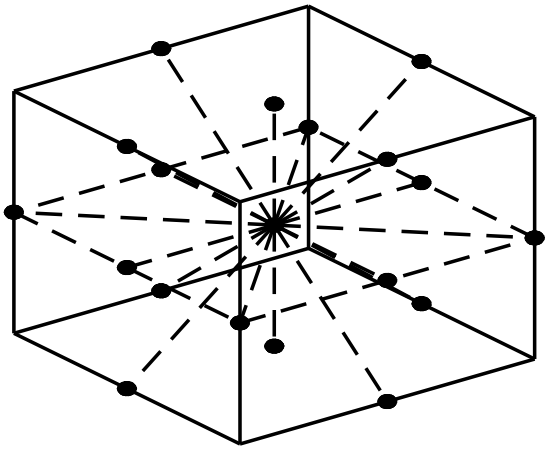

Fig. 4.1 The D3Q19 setup for the lattice domain. Note that the mid points are used for this particular setup rather than the corners, which would be the case for D3Q15, another common setup for 3D.

Eq. (4.3) is the main workhorse in LBM, and the correct distribution function must be established to solve different types of problems. For diffusion specifically, it can be shown (Mohamad 2011) that the equilibrium function is given by Eq. (4.5):

$$f_i^{eq} = \phi\omega_i \tag{4.5}$$

where ϕ is the concentration, and ω is a weighting factor in the *i* direction. The weighting factor will always sum to unity. To show that this solution corresponds to the diffusion equation, one can use the Chapman-Enskog expansion, which relates the meso-scale Lattice Boltzmann equation to the macroscopic diffusion equation and deduces how the relaxation parameter τ_r is related to the diffusion coefficient.

Utilizing the Chapman-Enskog expansion, the distribution function can be expanded in terms of some small parameter ε, as:

$$f_i(x, t) = f_i^0 + \varepsilon f_i^1 + \varepsilon^2 f_i^2 + \cdots \tag{4.6}$$

where f_i^0 is the distribution function at equilibrium, equal to f_i^{eq}. Summing the above equation for the *i* directions it can be shown that the higher order terms (1, 2, …) sum to zero (Mohamad 2011).

Further, expansion of the discretized distribution function using a Taylor series and substituting this into Eq. (4.4) while retaining the terms of order ε^2 and some mathematical manipulations gives:

$$-\frac{1}{\tau_r} f_i^2 = \frac{\partial f_i^0}{\partial t} - \tau_r \frac{\partial^2 f_i^0}{\partial x^2} c_i c_i + \frac{\Delta t}{2} \frac{\partial^2 f_i^0}{\partial x^2} c_i c_i \tag{4.7}$$

To recover the diffusion equation, Eq. (2.2), the equation above is summed over all directions *i* to yield the following:

$$\frac{\partial \phi}{\partial t} = \left(\tau_r - \frac{\Delta t}{2}\right) \frac{\partial^2 \phi}{\partial x^2} \tag{4.8}$$

A comparison of Eq. (2.2) and Eq. (4.8) shows the relationship between the Boltzmann equation and the continuum description of the diffusion equation, and that the diffusion coefficient is obtained as:

$$D = \tau_r - \frac{\Delta t}{2} \tag{4.9}$$

4.1.1 Lattice Boltzmann simulations and boundary conditions

LBM was used to solve the diffusion equation Eq. (4.10) for prescribed initial and boundary concentrations of the wood structure:

$$\frac{\partial C}{\partial t} = D_0 \nabla^2 C \tag{4.10}$$

where C is the concentration`, and D_0 is the free diffusion coefficient in the open pore space. A zero normal flux boundary condition was implemented at all walls in the structure, i.e. walls were considered to be impermeable. The zero-flux condition was then applied for curved boundaries according to:

$$-D_0 \frac{\partial C}{\partial n} = 0 \tag{4.11}$$

where n is the outward unit normal. The boundary condition was implemented with the use of ghost nodes, according to the methodology presented by (Gebäck and Heintz 2014). In contrast to the classical bounce-back rule applied for boundaries, the ghost nodes produced an accurate tangential flux near the surface by interpolating macroscopic values with a mirror point inside the domain that was based on the normal direction of the surface geometry.

The diffusion equation was solved until steady state, and the effective diffusion coefficient was obtained from the average flux as:

$$\overline{J_x} = -D_{eff} \frac{\Delta C}{\Delta x} \tag{4.12}$$

where Δx is the thickness of the simulation box, ΔC is the applied concentration difference, and $\overline{J_x}$ is the average flux in the direction of the concentration gradient. The simulation box consisted

of a uniform grid of lattice nodes set up in the D3Q19 domain, and a two-relaxation-time method for diffusion (Ginzburg 2005) was used, which benefits from improved stability while being equal in terms of both computation time and simplicity compared to the classical BGK approximation.

4.2 Geometry and models of the bordered pit

Due to the small scale of the structure of a pit, experimental measurements are extremely hard to perform to get accurate data on the flow or diffusion through a single bordered pit. Stamm (1946) has derived a model for diffusion through a cellular structure analogous to electrical conductance with resistance in series according to various wood structures, such as lumens, cell walls, and the interior of the pit. Petty (1973) has further developed said model for gases in dry wood to investigate the diffusion coefficient of bordered pits based on new data for structure and permeability in conifer wood. With recent advances in computing and simulation efforts, it has been proven possible to create high resolution models of a bordered pit, as done by (Schulte 2012; Schulte et al. 2015) for flow simulations in which the membrane structure of the margo is based on scanning electron microscope (SEM) images. This creates a realistic model of the structure. A similar approach was used in the present research.

The margo was based on a SEM image of an earlywood bordered pit by Petty (1972), shown in Fig. 4.2. Detailed resolution was obtained through vectorization of the image, after which the obtained vector image was extruded into 3D cylinders using AutoCAD.

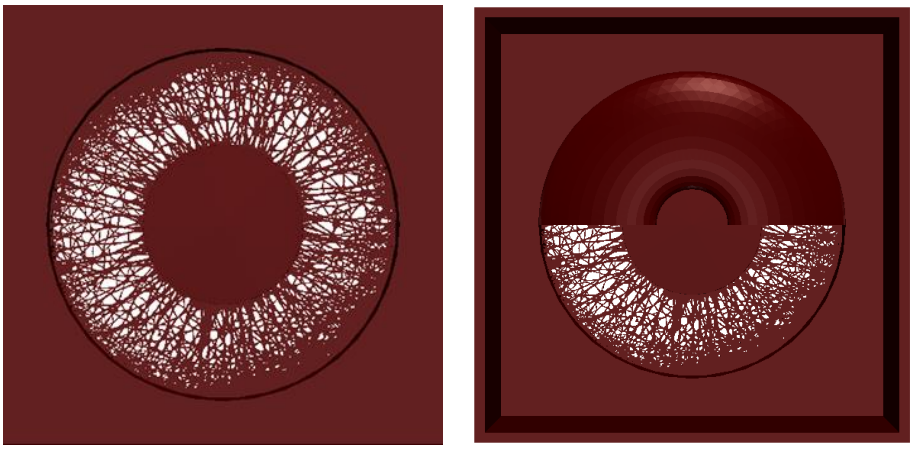

Fig. 4.2 To the left, vector representation of the margo extruded into three dimensions based on (Petty 1972). To the right, including borders and simulations box. The borders have been partially removed for illustrative purposes.

Additionally, the chamber and borders covering the membrane-like structure of the margo and torus were drawn up based on the average dimensions found in Table 4.1, seen to the right in Fig. 4.2. The depth, width, and height of the simulation box surrounding the pit were 12, 20, 20 μm.

Table 4.1 Dimensions of the pit components used to generate the geometry. Based on data from (Petty 1972; Siau 1984; Hacke et al. 2004; Trtik et al. 2007; Schulte 2012; Schulte et al. 2015).

Pit component dimension	Size (µm)
Margo thickness	0.05
Torus thickness (center)	0.50
Torus diameter	7.45
Margo outer diameter	16.10
Aperture diameter	3.70
Aperture depth	0.63
Chamber depth	1.98

To determine the resistance of each individual component of the pit, five different models/geometries were used as shown in Fig. 4.3. Model A in the figure represents the entire pit with borders, margo, and torus intact. Models B, C, and D in the figure are without the margo, torus, and borders, respectively. This allows for a direct comparison to determine the relative resistance between the models and, thus, the individual resistance of the borders, margo, and torus.

Model E was developed to simulate the effect that steam explosion may have on the structure of a pit. In that model, it is assumed that the treatment has opened or ruptured the borders, and the margo and torus have been removed.

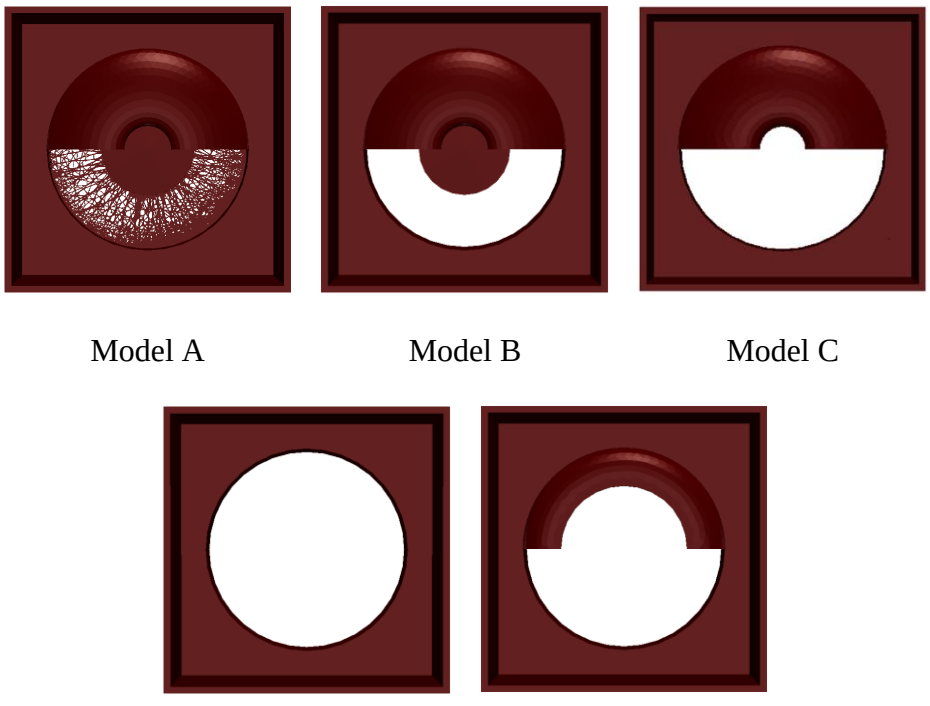

Fig. 4.3 The different models used in LBM simulations. Borders have been partially removed for illustrative purposes. Model A is the full model with borders, margo, and torus. Models B-D have had the margo, torus, and borders, respectively, removed to assess individual resistances relative to Model A. Model E represents a pit that has undergone steam explosion in which parts of the structure have been removed and the borders have detached somewhat.

4.3 Models based on X-ray tomography images

Reconstruction of tomography images into 3D structures for simulations has become increasingly more relevant as both the imaging techniques and simulation algorithms become increasingly sophisticated (Maire 2012). LBM has been shown to handle porous structures particularly well, and it has recently (Wassén et al. 2014; Gebäck et al. 2015; Eshghinejadfard et al. 2016; Guo et al. 2016; Liu and Wu 2016; Xia 2016; Zhang et al. 2016b, a) been used to simulate several different types of problems in 3D-generated structures based on tomography images.

4.3.1 Regions of interest and sub-volumes

To use the entire domain of the samples analyzed for simulation would be immensely computationally heavy, and, for this reason, smaller sub-volumes were investigated. To avoid any surface effects caused by sample preparation, only the center of the volume (where possible) was considered, as illustrated in Fig. 4.4.

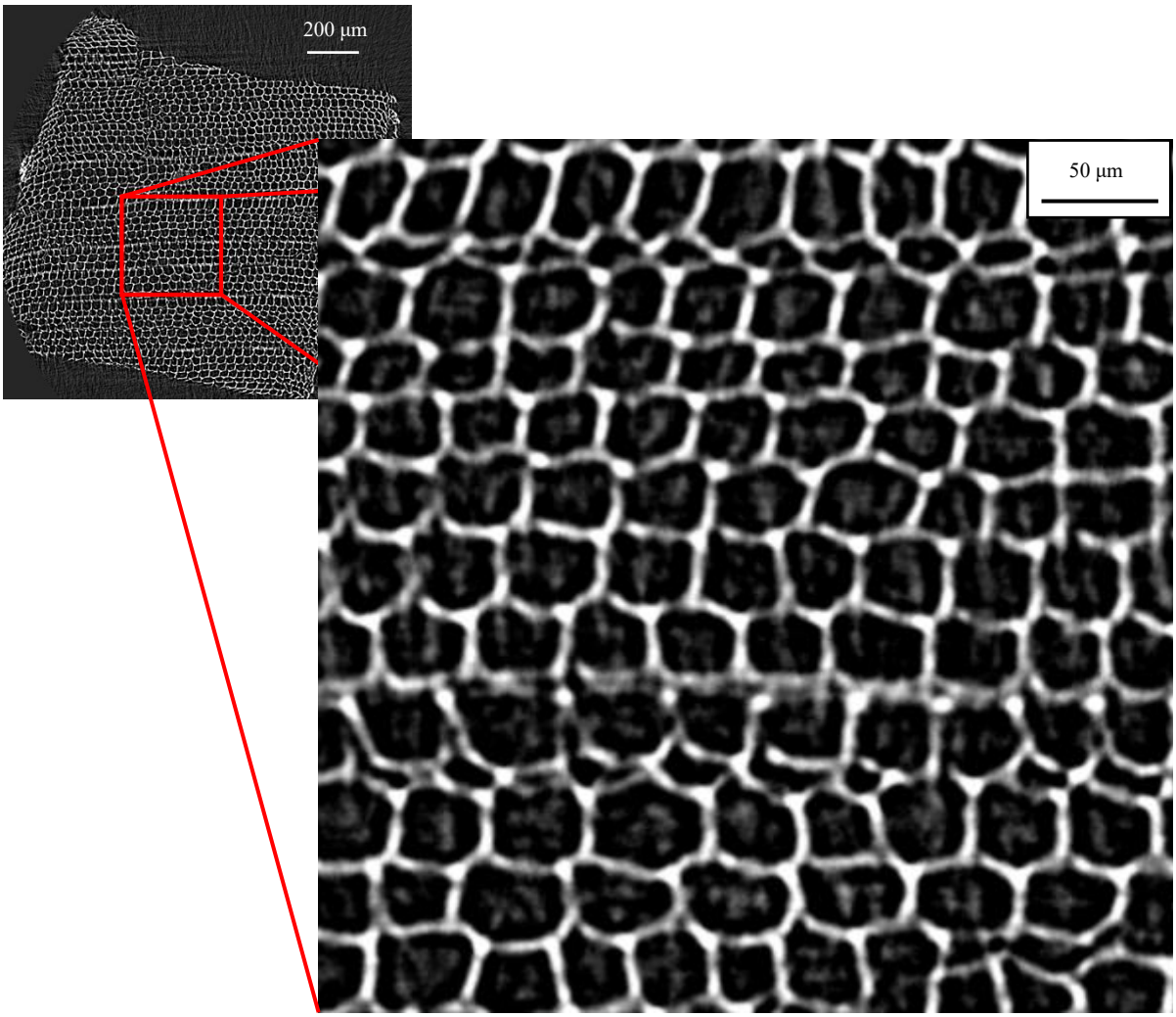

Fig. 4.4 Image obtained from the X-ray data for native wood. The highlighted area shows the image in full quality before any image processing. The size of the cropped image is 393 x 361 µm.

The SE-2 sample can be seen in Fig 4.5. This sample was highly variable in all spatial dimensions. To choose comparable volumes in the irregular structure is difficult if the open pore space between the separated cell walls is too large. As such, the sub-volumes were selected to encompass as much of the cell wall structure as possible while still including some of the separation, deeper into the sample. The three sub-volumes and their corresponding region of interest can be seen in Fig. 4.5.

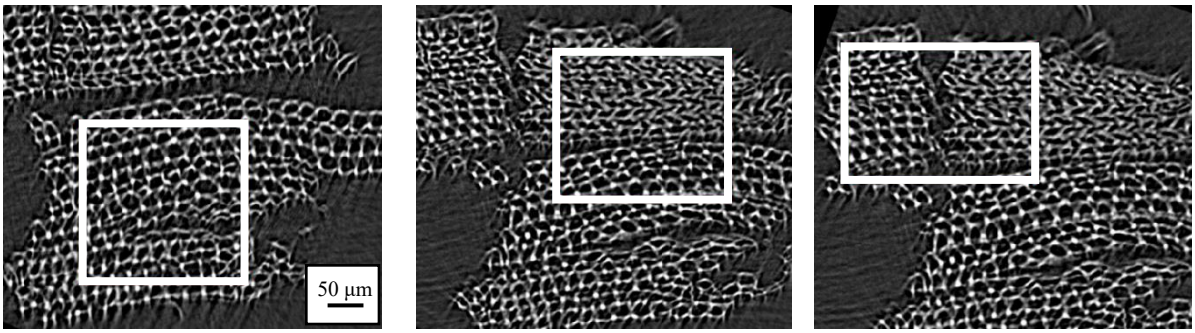

Fig. 4.5 Steam-exploded SE-2 sample from X-ray tomography. Solid lines indicate the sub-volumes.

4.3.2 Image processing and 3D reconstruction

It is necessary to process X-ray tomographic images before reconstructing a suitable geometry for performing numerical simulations. The main programs used for processing in the present research were ImageJ (version 1.51j) (Schneider et al. 2012) and MATLAB (The MathWorks, Inc., Natick, MA). The main processing concerns were removing background noise and artefacts while preserving the integrity of the sample structure. A Gaussian filter with $\sigma = 1$ was used to reduce jagged edges and to obtain a smooth surface of the geometry suitable for LBM simulations. A marching tetrahedral method (implemented in the GTS library, version 0.7.6, http://gts.sourceforge.net) was used to create a triangulated isosurface at a given threshold level. The isosurface was obtained in the form of an STL file.

4.3.3 Porosity, pore size, and tortuosity

Porosity was taken as the available fluid volume fraction in a simulation box. A simulation box spans the entire generated 3D geometry based on the STL file that defines the boundaries of the cell wall, and the available voxels in the open pore space are known. Pore size distribution was calculated by fitting spheres in the image stack from the X-ray data with the Thickness plugin in the BoneJ (version 1.4.2) (Doube et al. 2010) extension for ImageJ. Multiple spheres were fitted into the open pore space until all voxels were covered. The smallest sphere used was 2 µm. Gamma probability distributions were fitted to the histogram of sphere diameters for the entire image stack.

The tortuosity was calculated as the physical distance traversed (ΔL) by a solute per the length of the medium (Δx), according to:

$$\tau = \frac{\Delta L}{\Delta x} \tag{4.13}$$

Using the obtained diffusive flux field from the LBM simulation, the distance traversed can be calculated as the streamlines of the flux vector field. To obtain an average value for the distance, streamlines were randomly sampled throughout the simulation domain for each sample. Calculations of tortuosity were performed in Matlab.

4.3.4 Multiscale implementation

An algorithm based on watershed segmentation and written in Matlab was used (Meyer 1994). The watershed transform is normally applied to separate objects touching in images. In the present case, it was used to separate the connecting tracheids and, thus, effectively find the location of a bordered pit. A cross-section of the voxel data was converted to a binary image, as seen in Fig. 4.6A. The Euclidean distance transform of the binary image was computed with the bwdist function in Matlab and, combined with extended-minima transform, produce Fig. 4.6B. These two transforms are useful for objects that are circular in shape and touch, ensuring that the watershed transform will not over segment the image. Last, the watershed transform was applied, and all tracheids were segmented, as seen in Fig. 4.6C.

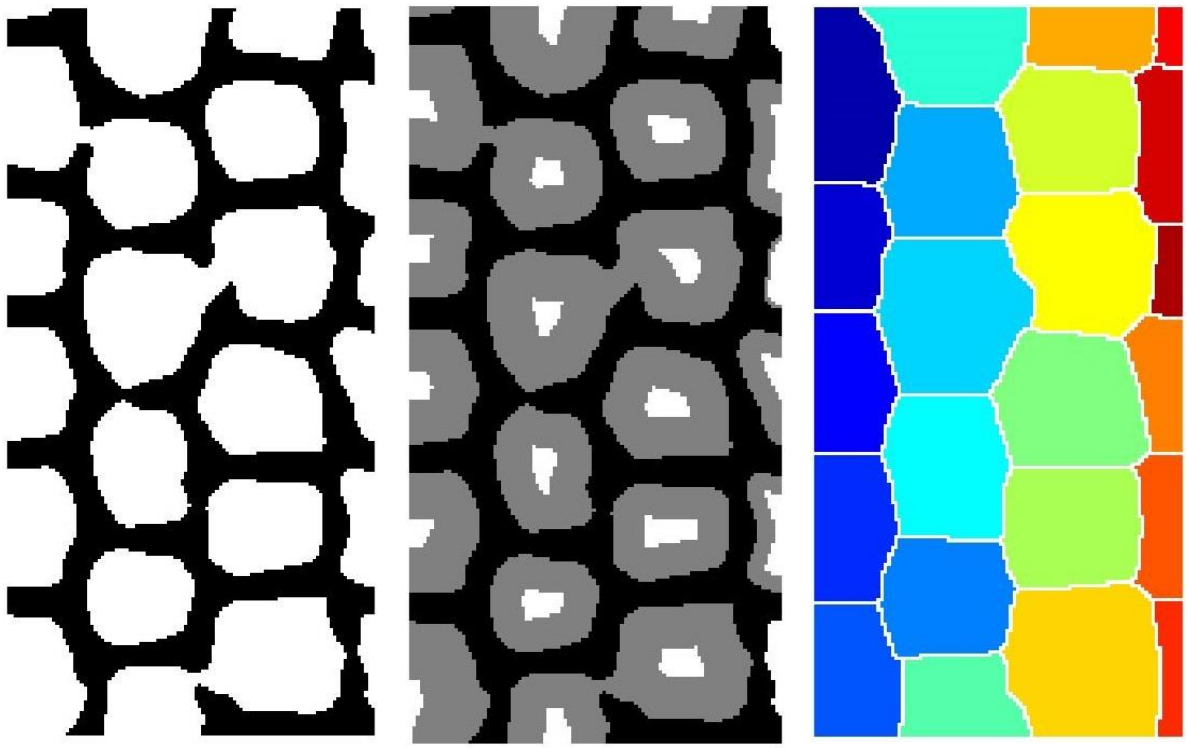

Fig. 4.6 Finding the spefic location of connectivity between the larger pores by using a watershed algoithm. Depicted in A is a cross-section of the larger data set, which has been converted to binary data. In B, Euclidean distance and extended-minima transforms have been applied to the binary image. C shows the application of the watershed transform.

The diffusion coefficient was then inserted into voxels surrounding the area found by the algorithm and the total space occupied by the pit could be obtained and varied, as illustrated in Fig. 4.7. After this had been implemented, diffusion simulations were run with the variable diffusion coefficients.

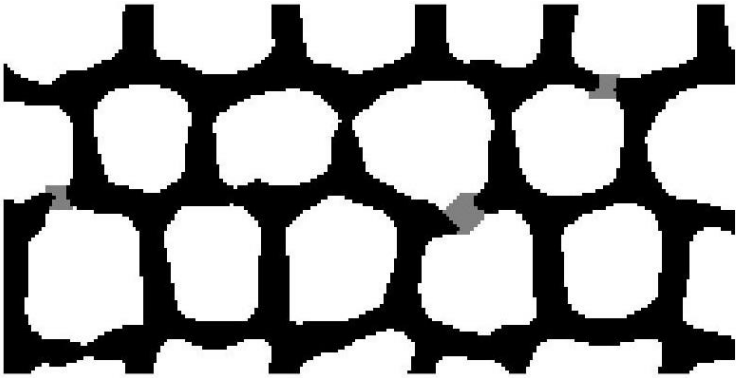

Fig. 4.7 Spatial locations of the variable diffusion coefficients supplied to the simulation. The cell wall (black) is zero, while the lumens (white) and bordered pits (gray) are supplied as ratios where the lowest is 1 (for the pit).

5 Results and Discussion

This section is divided based on the findings of the four papers. First, the local diffusion measurements performed with FRAP will be summarized based on Paper II. After this, the results of the first two simulation studies regarding diffusion through bordered pits (Paper I) and diffusion in the microstructure (Paper III) are presented. Last, multi-scale modeling results (Paper IV) that connect the results from Papers I and III are presented.

5.1 Experimental results

This section mainly covers the results obtained from the experimental study in Paper II.

5.1.1 Free diffusion coefficient in solution

Two diffusion probes were used with varied molecular weight to represent what may be relevant for a materials biorefinery. The first was the polysaccharide dextran chosen to represent large biopolymers present in wood, such as hemicelluloses. The second was a globular protein, chosen to represent enzymes relevant for wood processing. Results for both probes can be seen in Table 5.1 below. Dextran, marked with the fluorophore FITC, diffusivity was measured using FRAP methodology, while the protein diffusivity was estimated theoretically from the Stokes-Einstein formulation.

As can be seen in Table 5.1, diffusion coefficients of the same molecular weight for the two probes differ significantly due to their hydrodynamic configuration. This was also seen in the hydrodynamic radius calculated based on the Stokes-Einstein equation where the dextran was more than twice as large as the protein.

The coefficients for dextran follow earlier experimental results from Arrio-Dupont et al. (1996) as well as the correlation produced by Sellen (1975). However, due to polydispersity, there is always some discrepancy in the results, especially at lower molecular weights. As polymers become larger the diffusion coefficient follows an inverse square root molecular weight dependency (Bird et al. 2007).

The free diffusion coefficients for the protein diffusion probes were calculated based on the minimum diameter for the given molecular weight with the Stokes-Einstein equation. The equation has some inherent uncertainties due to the assumptions behind it, such as a perfectly smooth spherical particle (Cussler 2009). Proteins have irregular surfaces (Erickson 2009) which means that the average diameter would be slightly larger than that assumed here.

Table 5.1 The free diffusion coefficient in a solution of dextran and protein probes. Equivalent radius is given as a comparison between the probes.

Diffusion probe	Molecular weight	Diffusion coefficient [$\mu m^2/s$]	Hydrodynamic radius [nm]
FITC-Dextran	3 kDa	154.3 ± 1.9	1.59 ± 0.02
	10 kDa	75.6 ± 1.3	3.25 ± 0.05
	40 kDa	42.6 ± 0.6	5.76 ± 0.08
Protein	40 kDa	109	2.26
	60 kDa	95	2.58
	80 kDa	86	2.84

5.1 Diffusion measurements in steam-exploded wood

The aim of Paper II was to assess diffusion coefficients locally of large molecules in steam-exploded wood and explore how well the FRAP methodology can be applied to microstructure in wood. Dextran marked with the fluorophore FITC was used throughout the experiments. A general setup for the FRAP measurements from the perspective of the microscope and the subsequent intensity data can be seen in Fig. 5.1 below.

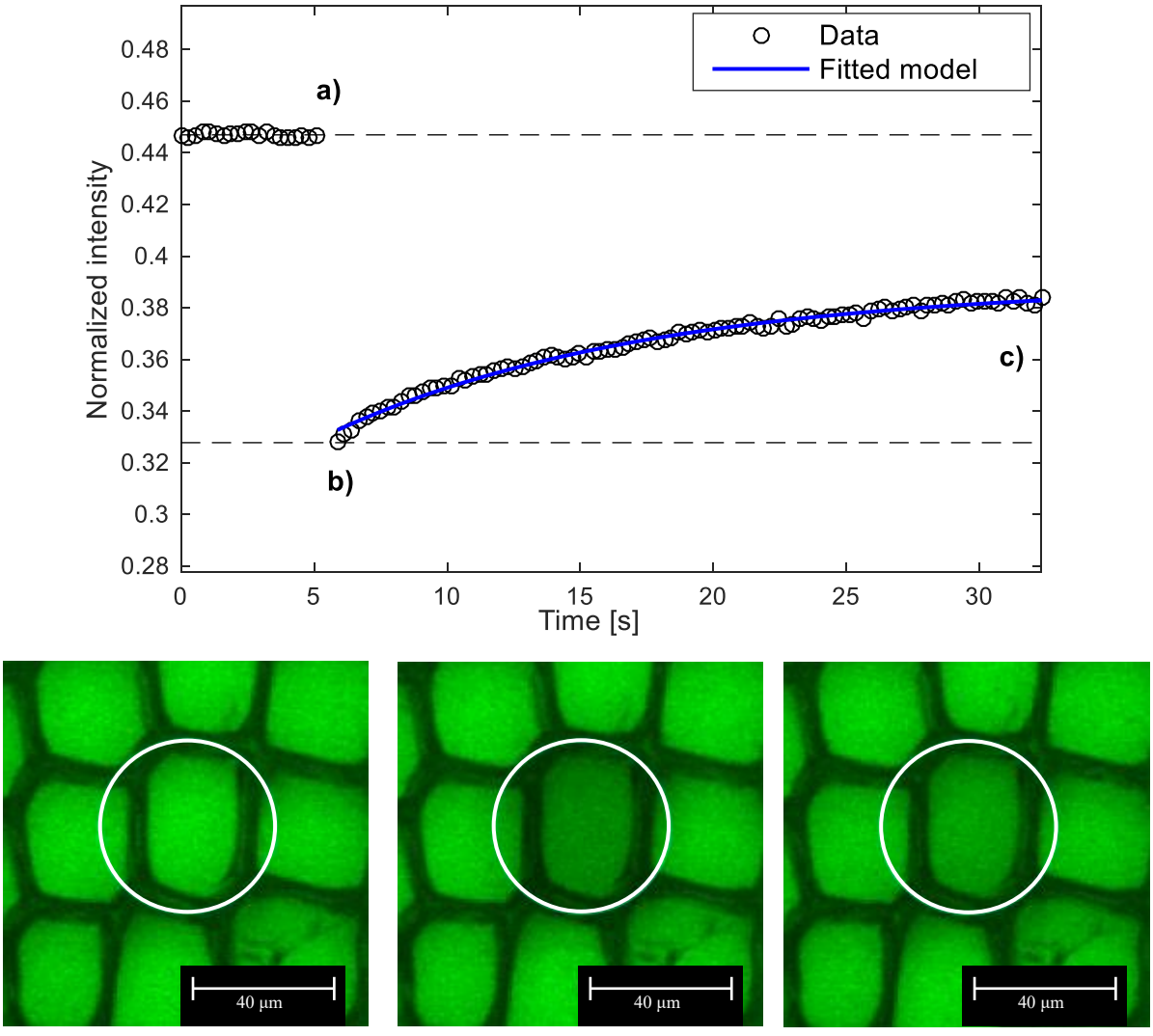

a) Pre-bleach **b)** Bleach **c)** Post-bleach

Fig. 5.1 A typical FRAP measurement with the 50 µm circular ROI for a lumen, including micrographs at 3 different time points as indicated in the recovery curve. Figure a) is pre-bleached and is indicated on the recovery curve before the drop, b) is just after the drop, and c) is at the end of the post-bleach.

The result for the 3 kDa dextran diffusion probe is presented in Fig. 5.2, based on the three different locations in the earlywood structure: adjacent to ray cells, at the interface between early- and latewood, and tracheids. The native samples were found to have the lowest diffusion coefficient while a subsequent increase was found for the SEW and SEIW samples. However, no significant difference was found for different locations in the structure.

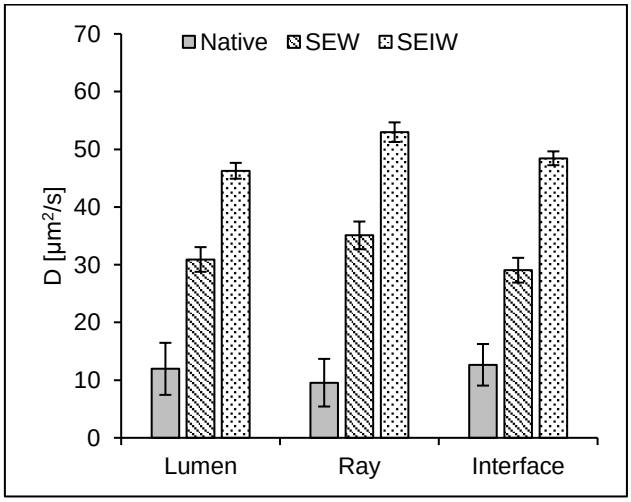

Fig. 5.2 Diffusion coefficients in µm^2/s for FITC-dextran of 3 kDa. The FRAP measurements were performed adjacent to ray parenchyma cells, the interface between early- and latewood, and lumens

Contrary to what was observed for the 3 kDa probe, no significant difference was found for the two larger probes among the wood samples, presented in Fig. 5.3. All three probes indicated no significant difference in radial diffusion due to adjacent microscopic structural elements.

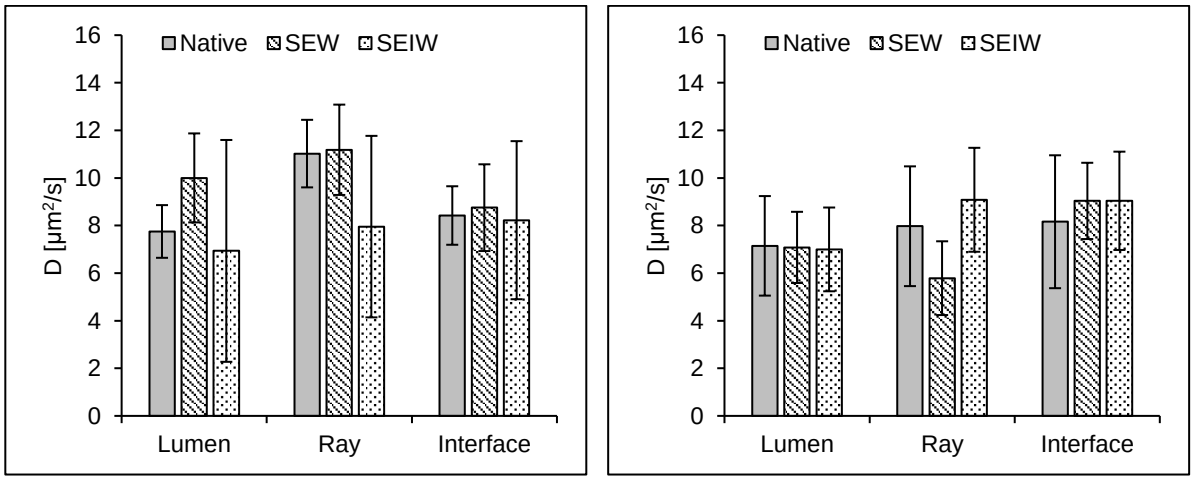

a) FITC-Dextran 40 kDa **b)** FITC-Dextran 10 kDa

Fig. 5.3 Diffusion coefficients in µm^2/s for FITC-dextran of 10 kDa and 40 kDa. The FRAP measurements were performed adjacent to ray parenchyma cells, the interface between early- and latewood, and lumens.

More severe structural changes in the form of ruptures in the microstructure occur during the impact step in steam explosion. One such case is presented in Fig. 5.4a where a rupture has

caused a separation between early- and latewood as well as damage to the cell walls. Measurements were performed around the separation for the largest dextran probe, enumerated in Fig. 5.4a.

In the large void caused by the separation, the diffusion coefficient approaches the free diffusion coefficient (1-4 in Fig. 5.4b), and the nearby cell walls have little to no effect, as expected. For nearby lumens close to the rupture (5-7 in Fig. 5.4b), the diffusion coefficient is lower, indicating that the probe is somewhat obstructed.

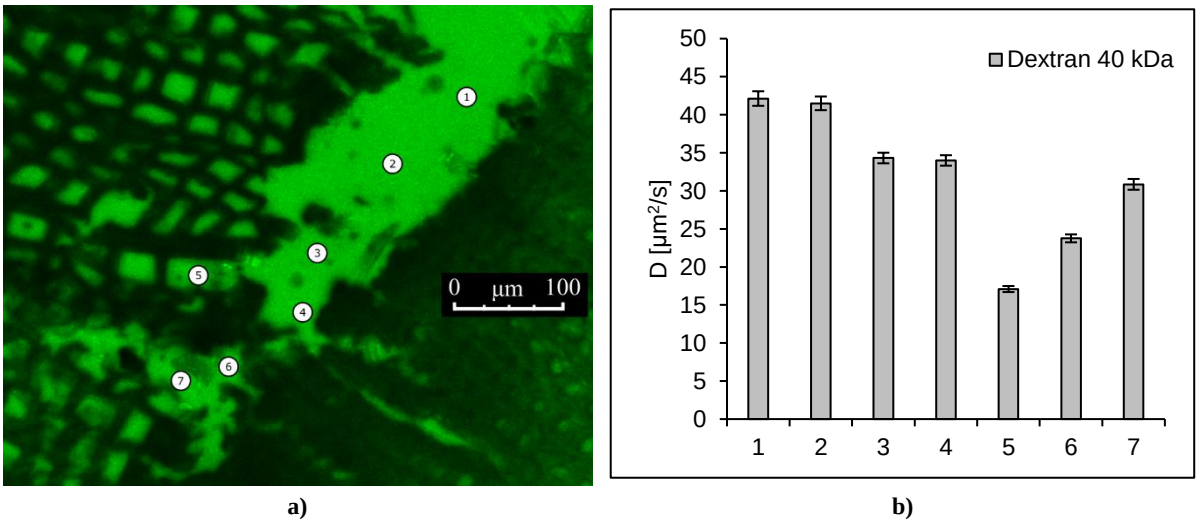

a) **b)**

Fig. 5.4 CLSM micrograph **a)** of SEIW sample. The rupture that occurred between the dense latewood, to the right, and earlywood to the left. FRAP measurements were performed at the enumerated circles (1-7) indicated on the micrograph. A circular ROI of 10 µm was used. In **b)** corresponding diffusion coefficients in $\mu m^2/s$ for FITC-dextran of 40 kDa. FRAP measurements were performed only on SEIW samples.

5.2 Simulation results

This section covers the main results from the diffusion simulations performed in Papers I, III, and IV. In Paper III, the microstructure of wood was resolved with X-ray tomography data, diffusion was simulated, and the local diffusion coefficient was computed. In the microstructure the bordered pits could not be resolved properly. Instead, a single pit was examined in detail in Paper I. Lastly, Paper IV combines the knowledge obtained from both Papers I and III in a multiscale model to include bordered pits in the microstructure model of wood.

All simulations were transient and solved until steady state with the impermeable boundary condition for the walls of the cell wall structure. A concentration difference was set for the inlet and outlet in a specified direction. The other directions used a periodic boundary condition.

5.2.1 Diffusion through bordered pits

Due to the small scale of the structure of a pit, it is very difficult to perform experimental measurements to get accurate data on a single bordered pit. In this work, we explore the possibility of resolving the entire pit by generating its structure from SEM images of the margo and reconstructing the geometry of a single bordered pit. The effective diffusion coefficient obtained at this scale will be used in the multiscale implementation presented in Section 5.2.4.

The effective diffusion coefficients calculated for the different models of the pits using LBM are presented in Fig. 5.5 and Fig. 5.6. The results have been scaled to exclude the simulation box such that the effective diffusion coefficient represents only the bordered pit.

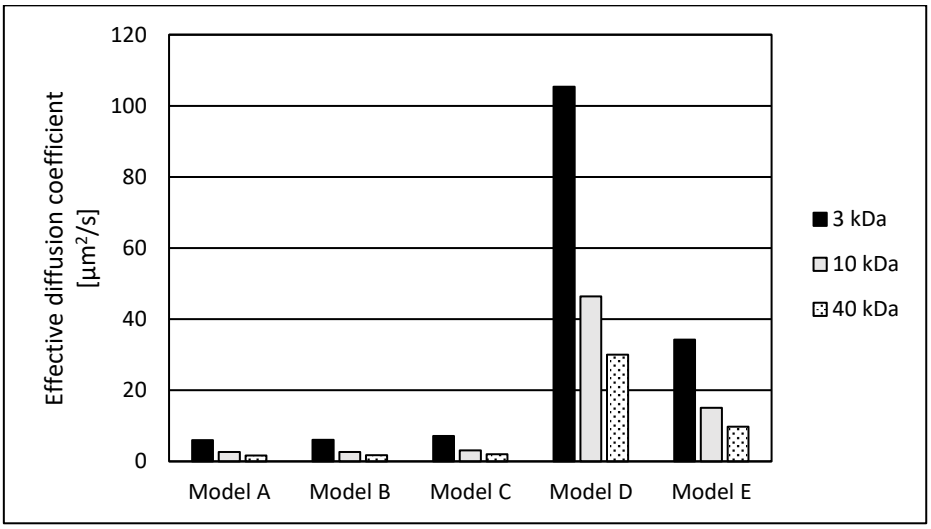

Fig. 5.5 Effective diffusion coefficients using the five LBM models and the dextran diffusion probes of 3, 10, and 40 kDa. The effective diffusion coefficient is given in µm²/s.

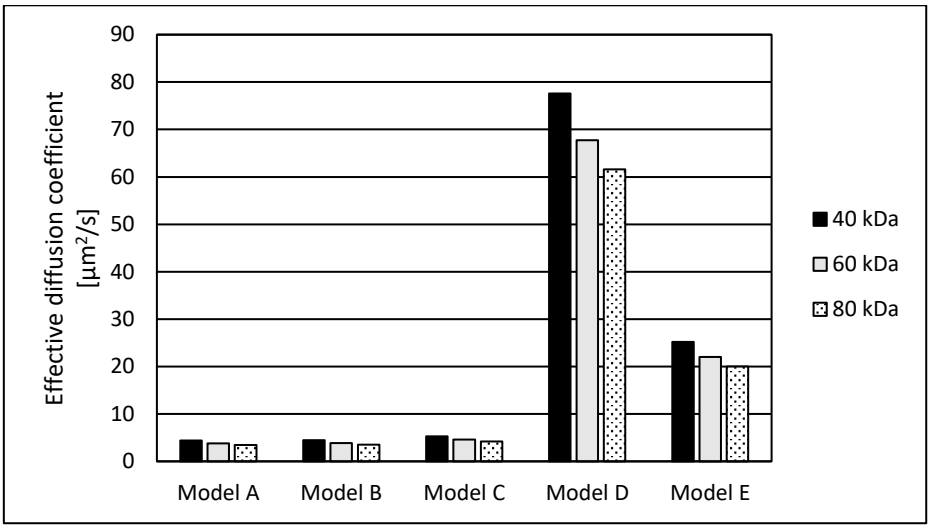

Fig. 5.6 Effective diffusion coefficients using the five LBM models and the calculated values for the proteins of 40, 60, and 80 kDa. The effective diffusion coefficient is given in µm²/s.

Three different results are shown in Fig. 5.5 and Fig. 5.6 according to the diffusion probe used to scale the results. The difference in coefficients between Models A and B is very small, which indicates that the margo did not hinder diffusion much at all. Model C shows a small increase because the torus was not present, and the path of diffusion was shorter. Without the borders present in Model D, a large increase in the diffusion coefficient can be seen due to the large increase in the cross-sectional area. While in Model E, where the borders had been deformed due to steam explosion but were still present, the increase is not as large as in Model D but still significantly higher than for Models A, B, and C.

To illustrate the path of diffusion for Model A, integrated flux lines from the LBM simulation, are shown in Fig. 5.7 for a cross-sectional slice.

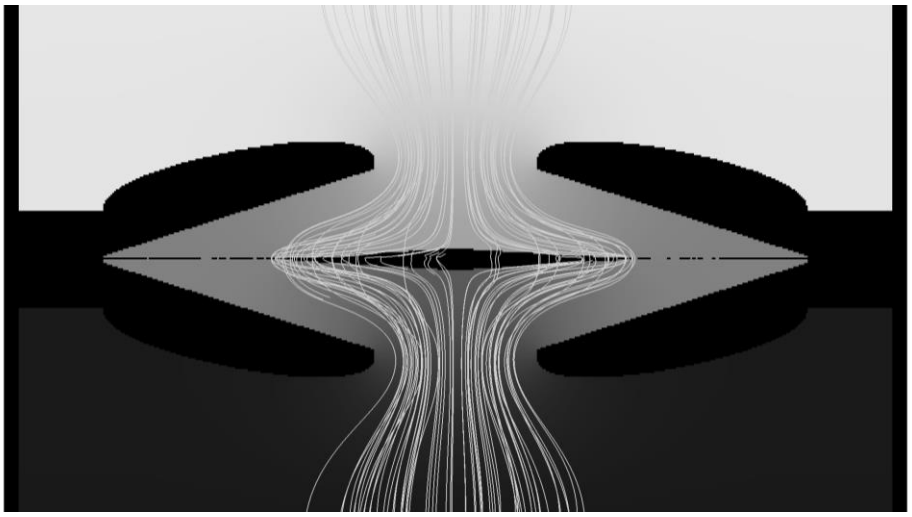

Fig. 5.7 A 2D cross-sectional slice of the simulations for Model A. The solid walls are shown in black while the concentration gradient is in gray scale where high concentration is darker and low concentration lighter. Integrated lines of the flux field are made visible through the structure based on a point source generated with the stream tracer filter in Paraview.

Based on the simulations of Models A and E, equations for the effective diffusion coefficient can be expressed for the entire undisturbed pit and the steam-exploded pit with the following equations as a function of the free diffusion coefficient:

$$D_{eff} = 0.040 D_0 \tag{5.1}$$

$$D_{eff,Stex} = 0.232 D_0 \tag{5.2}$$

Schulte (2012) and Schulte et al. (2015) have modelled water flow through bordered pits and reported that the margo and torus together constitute more than 80 % of the flow resistance. Valli et al. (2002) have ascribed 38 % of the flow resistance to the margo. The membrane resistance to diffusion was found to be close to 2 % in the present work. The large difference between flow and diffusion resistance is explained by the presence of shear stresses in the flow and the large surface area of the thin-stranded membrane structure of the margo; while for diffusion, the available cross-sectional area and length of the margo pores control resistance. Note that, for diffusion, the presence of a structure does not influence the tangential flux along the structure; while for flow, the no-slip boundary condition imposes zero tangential velocity at the structure boundary, which has a major effect on flow resistance, especially in narrow channels.

5.2.2 Diffusion in the microstructure of wood

The microstructure of native and steam-exploded wood was resolved with the use of X-ray tomography images with subsequent simulations of diffusion using LBM. The simulations were solved until steady state was reached after which the effective diffusion coefficient was calculated. Steady state results are presented in this section as the ratio of the effective- over the free diffusion coefficient. This yields a geometry factor, i.e. a measure of how the structure retards diffusion.

Transient results were investigated to study the evolution of the concentration front over time to obtain information on diffusion pathways and how long it takes for diffusing solutes to traverse the porous structure being studied. Since the simulation was performed with dimensionless variables, the free diffusion coefficient of 40 kDa FITC-dextran was used to obtain the time scale.

The concentration front for the native wood moved significantly slower than the front for wood pretreated with steam explosion, as seen in Fig. 5.8 and Fig. 5.9. Diffusion between tracheids was through bordered pits in the native wood, and transport depended heavily on connectivity. Additional connectivity was seen for steam-exploded samples due to the degree of disintegration. If a sample that has undergone steam explosion in any way ruptures and opens up, an increase in the connectivity between tracheids will be seen, and diffusion will significantly increase.

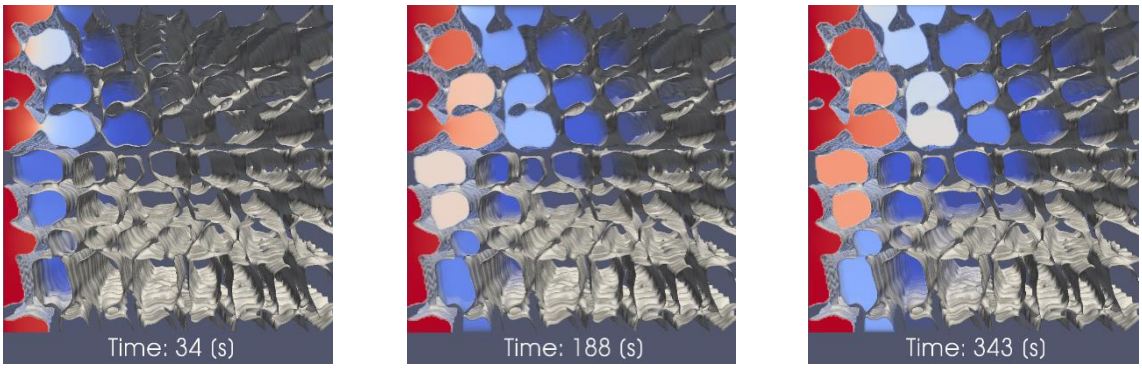

Fig. 5.8 Time evolution of the concentration front in the native sample. Diffusion is limited by the connectivity of the bordered pit between tracheids. An initial constant concentration is applied at the left-most side in the simulation box (shown in red) at time zero.

The transversal diffusion in different sub-volumes within the native sample behaved similar to what is shown in Fig. 5.8. The concentration front moved slowly from tracheid to tracheid through the bordered pit openings. A similar result was observed for the SE-1 sample. However, in certain regions of the SE-1 sample, where the connectivity was greater, the front progressed faster and spread out more quickly.

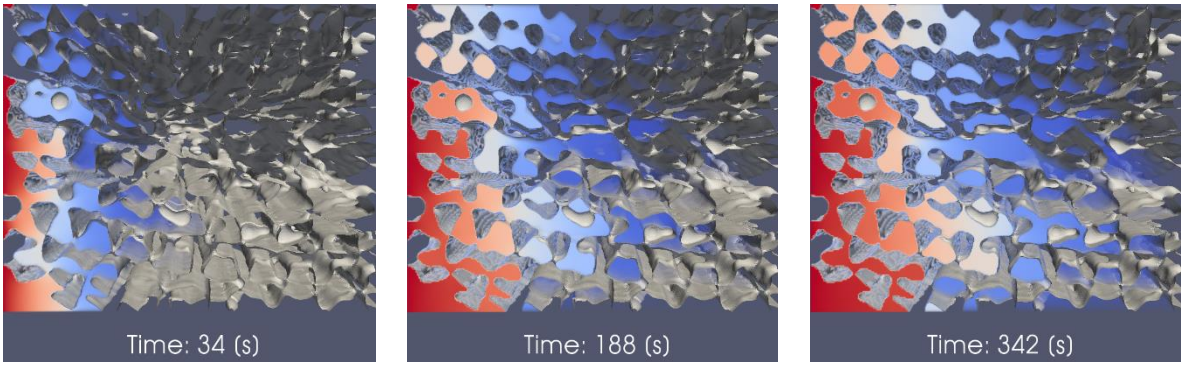

Fig. 5.9 Time evolution of the concentration front for a steam-exploded sample. The increase in connectivity affects the path of diffusion, and, thus, the time it takes for the concentration to progress over the sample can clearly be seen. An initial constant concentration is applied at the left-most side in the simulation box (shown in red) at time zero.

Observations of the concentration over time in the SE-2 samples revealed an increase in the diffusion rate throughout the structure, as was expected. Even though the pore sizes of the SE-2 sample was smaller, due to the structure being compressed by collisions, the increase in connectivity was significant, which leads to a much smoother concentration profile in the exploded sample compared to the native one.

Diffusion in wood is highly directional-dependent, and in the longitudinal direction, along the fibers, diffusion takes place many times faster. In the transversal direction, diffusion occurs from lumen to lumen via bordered pits. The pit openings are significantly smaller than the lumina and act as a large obstacle to diffusion, which is clearly seen in Fig. 5.10. The pits in the present simulations could not be resolved and was completely open, i.e. no pit aspiration. Due to the small size of the torus it is unlikely that the aspiration of pits can be properly considered with this method. Because of this and the fact that the aperture of the pits is of variable size, up to that of the inner diameter of the margo, the diffusion coefficient should be somewhat inflated. Another effect may be the filtering of large molecules through the fine pores in the margo. These effects were not considered in the present model.

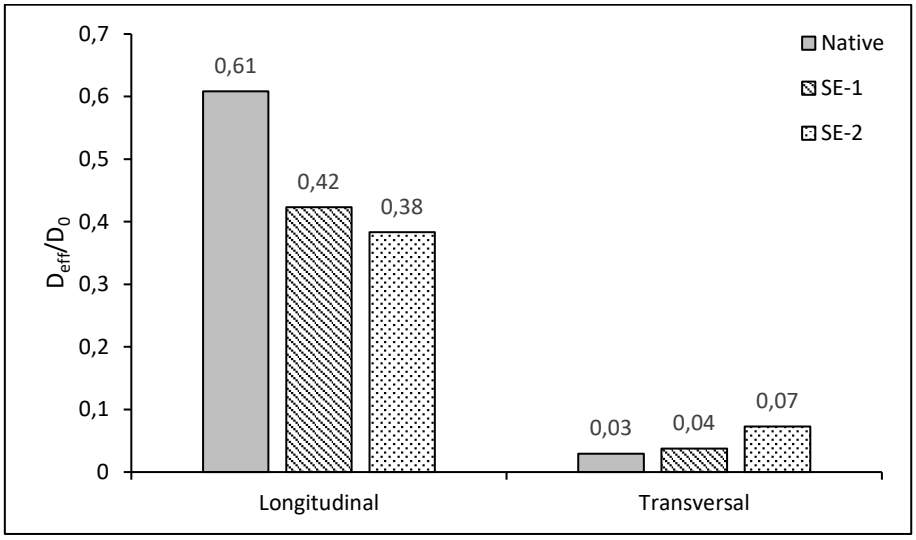

Fig. 5.10 The ratio of effective diffusivity over free diffusivity in the longitudinal direction and in the transversal direction of the three samples.

The release of pressure during steam explosion causes an expansion of vapor within the structure of a sample and is known to increase porosity (Muzamal et al. 2015) in pores with diameters of less than two micrometers. Due to the limitations of tomography imaging, it is hard to capture these small changes, which is reflected in similar results for the native and SE-1 samples in Fig. 5.11. It is difficult to see a microscale difference in diffusion due to this, however, for nano-scale phenomena, such as enzyme binding and penetration inside the cell wall, this is of great importance as has been shown in (Azhar et al. 2011; Jedvert et al. 2012b; Muzamal et al. 2016).

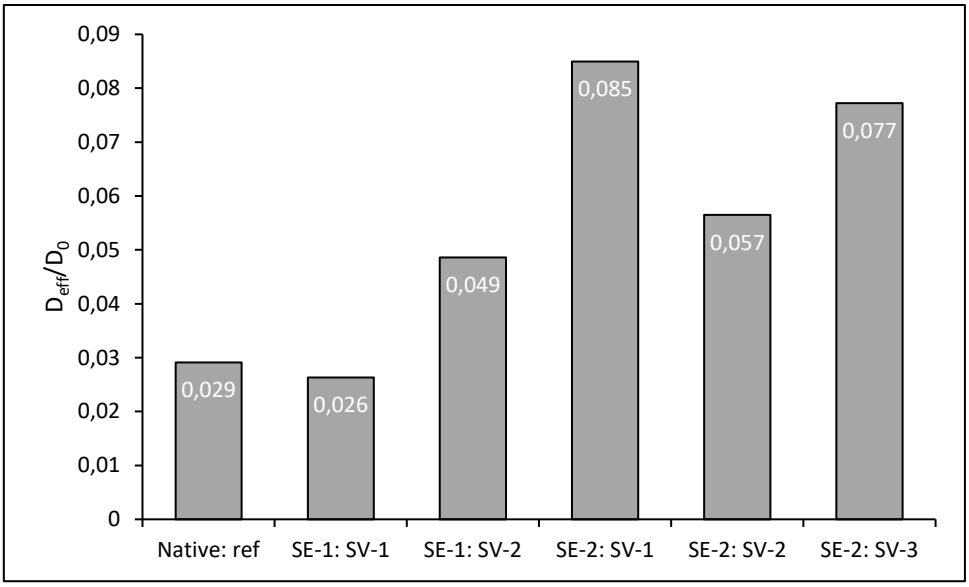

Fig. 5.11 The ratio of effective diffusivity over free diffusivity for different regions of interest for native wood and two steam-exploded wood samples. The native sample had only one sub-volume (ref), and the steam-exploded samples (SE-1 and SE-2) had two and three sub-volumes (SV-1 to SV-3), respectively.

In a study on the diffusion of polyethylene glycol in native Sitka spruce, Fukuyama and Hiroyuki (1986) have reported values of radial diffusivity (D_{eff}/D_0) from 0.0091 to 0.0032 for increasing molecular weight. Similarly, they have reported values of 0.478 to 0.222 for the longitudinal direction. The coefficients based on the simulations for native wood in Fig. 5.10 are somewhat lower for the longitudinal while for the transversal direction, the coefficients are about one order of magnitude lower than what was reported by Fukuyama and Hiroyuki (1986). This is both an effect of comparing experiments performed at the cm scale with simulations at the μm scale, as well as not resolving the refractory nature of the pits.

The measurements performed using FRAP were over single tracheids in the transversal direction, and values of D_{eff}/D_0 for a 3 kDa FITC-dextran probe were the following: for the native sample, 0.067; for the SEW sample, 0.20; and for the SEIW, 0.33. The FRAP data for the pretreated samples was vastly different from the simulated data; it was highly dependent on the local tracheid chosen and how it was affected. However, the values for the native sample were of the same order of magnitude as the values from the simulations.

5.2.3 Porosity, pore size, and tortuosity

Calculated tortuosities and porosities for the corresponding pore size distributions of the samples can be seen in Fig. 5.12 and Fig. 5.13. The choice of sub-volume region and size are of importance and should be consistent between samples to obtain comparable values for porosity and tortuosity. The native sample had the highest porosity of all the samples. Pore sizes were found to decrease for the pretreated samples, especially for SE-2, as the choice of sub-volume for SE-2 mainly encompassed the compacted micro-structure caused by collisions of the wood sample after pressure release. If the entire samples were analyzed, the large cracks and ruptures of the cell walls would increase pore size significantly. In a study by Zauer et al. (2014), a decrease in the pore size of thermally treated wood was found. Similarly, Van den

Bulcke et al. (2013) have shown that aspen wood thermally treated at 160 °C shrinks, but the overall wood microstructure remains the same.

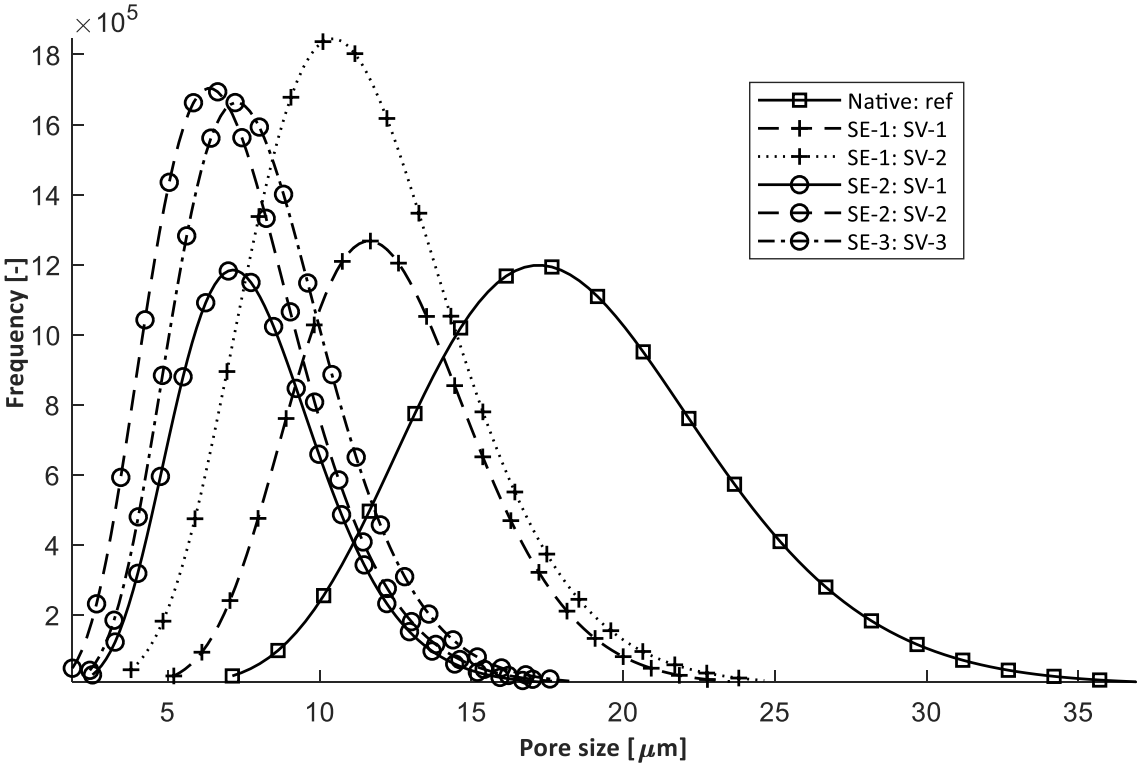

Fig. 5.12 Pore size distributions for native (square), SE-1 (plus sign), and SE-2 (circle) samples. Gamma probability distributions have been fitted to the pore size histograms.

The only noticeable effect of the pretreatment on the SE-1 sub-volumes is the lower tortuosity for SV-2, seen in Fig. 5.13. The lower tortuosity for SV-2 seemingly has more of an influence than porosity on the effective diffusion coefficient, as the porosity is also lower for SV-2. In a previous study by Muzamal et al. (2015), an increase in small pores in the range of 1 – 5 µm for steam-exploded wood was found using mercury porosimetry. The increase in smaller pore sizes and the effect of thermal treatment may explain the relative decrease in porosity for the steam-exploded samples in this study, especially since the samples are local volumes and are not representative of the entire sample obtained after steam explosion.

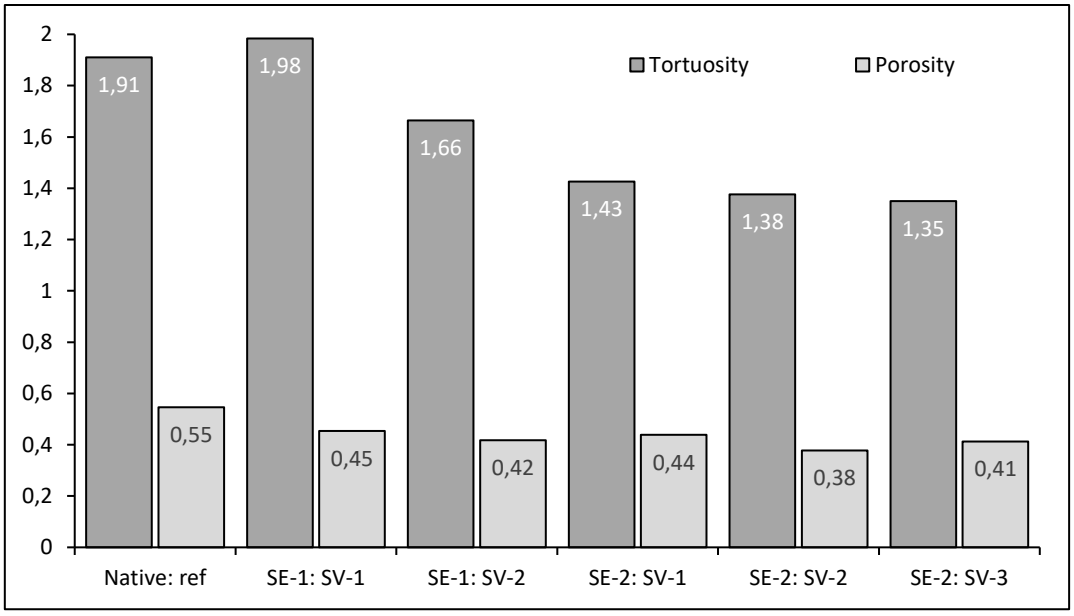

Fig. 5.13 Porosity and tortuosity for all samples. Porosity was obtained from the available fluid volume fraction and tortuosity was obtained by random sampling of streamlines in the flux field.

Although the porosity reported in Fig. 5.13 is lower than the published values close to 0.7 (Plötze and Niemz 2010; Zauer et al. 2013) it must be taken into account that this is a local average and not a macroscopic average. Also reported in Plötze and Niemz (2010) is the large number of nano-pores present in spruce wood that cannot be resolved with the present methodology. The general trend we observed was that native wood had a greater porosity and tortuosity, which indicates that, although more pore space was available for diffusion, the path was longer.

Another effect that lowered both pore size distribution and porosity was the delineation of the cell wall. Reported average cell wall thickness values of Norway spruce are 3.52 µm and 2.90 µm in the radial and tangential directions (Brändström 2002), respectively, while even values as low as 2.1-2.2 µm have been reported by Havimo et al. (2008) for cell wall thickness in the tangential direction. Measurements of micrographs of a native wood sample taken with a confocal microscope yielded a cell wall thickness of 3-4 µm. Measurements of the tomography scans of the native samples resulted in an average cell wall thickness of 4.80 - 6.48 µm in the radial and tangential directions, respectively. The high value in the tangential direction is due to ray cells being resolved as cell walls. This factor, in combination with the smoothing using Gaussian filters, overestimated cell wall thickness. Filters that preserve edges, such as bilateral or anisotropic diffusion, can be used to avoid loss in sharpness. However, smoothing was necessary for both noise removal and to obtain a smooth surface such that the boundary condition could be applied accurately.

5.2.4 Multiscale diffusion – Bridging the scales

Multiscale modeling was employed to overcome the difference in scale when resolving a bordered pit in detail and, at the same time, resolving the microscale of tracheid to tracheid diffusion. This modeling is also beneficial for the limitations in resolution of X-ray tomography, the resolution of which is not high enough to resolve pits. However, even if a tomography

technique could resolve the pits in detail, the computational demand of simulating only a few tracheids would quickly become too much to handle.

The geometries used in the multiscale study are presented in Table 5.2. Compared to the previous models of the microstructure, more care was taken to avoid ray cells.

Table 5.2 Summarized information regarding the four generated surfaces including porosity, number of pits, and the equivalent diameter of the pits based on a sphere with the same volume.

Geometry	Porosity	Number of Pits	Equivalent Diameter of Pits (μm)
Case 1:	0.620	29	7.5 ± 2.2
Case 2:	0.632	39	7.2 ± 2.6
Case 3:	0.644	44	7.5 ± 2.6
Case 4:	0.656	43	8.0 ± 2.8

The cell wall thickness in the radial and tangential directions was, on average 4.6 μm, with an increase in the cell corner. Published data on Norway spruce cell wall thickness ranges from 2.10 – 3.52 μm (Brändström 2001; Havimo et al. 2008). The larger cell wall thickness leads to a somewhat lower porosity than expected for earlywood (about 0.7 for the bulk, including cell wall porosity (Plötze and Niemz 2010; Zauer et al. 2013)). However, increasing the image threshold further to decrease cell wall thickness would compromise the structure around the pits because of intensity variations. Case 4 seems to be the limit for this image data for pushing porosity while keeping the diameter of the pits within the calculated average for a softwood pit of 7.6 μm.

The average length of a softwood tracheid is 2 – 4 mm, and each tracheid contains, on average, about 200 bordered pits (Sjöström 1993). Assuming an average and not accounting for increased pit density towards the end of the tracheid (Brändström 2001), we can expect around 13 pits per 200 μm of length. The geometry in this study was 162 μm long, and covered about 12 tracheids, giving 6 pairs and a reasonable number of pits around 50. Both the size and number of bordered pits are reasonable when compared to the average data found in the literature.

The computed effective diffusion coefficients based on LBM simulations are shown in Fig. 5.14 and Fig. 5.15. The variable diffusion coefficient in this figure is represented by ratios, and in the first 1:1, the same diffusion coefficient is used for both the lumina and pits, i.e. no multiscale implementation. For the other three simulations, the open space within the pits was scaled at a ratio according to 1:2, 1:4, and 1:10. Effectively, this means that the coefficient in the lumina is 2, 4, and 10 times larger than that of the bordered pits. The lower limit for an undisturbed pit in untreated native wood is 1:25; however, due to numerical stability issues in the simulations, such a large difference could not be simulated. The different ratios represent different degrees of opening or rupturing of the bordered pit caused by steam explosion, where 1:1 would represent a bordered pit where the borders had been completely removed.

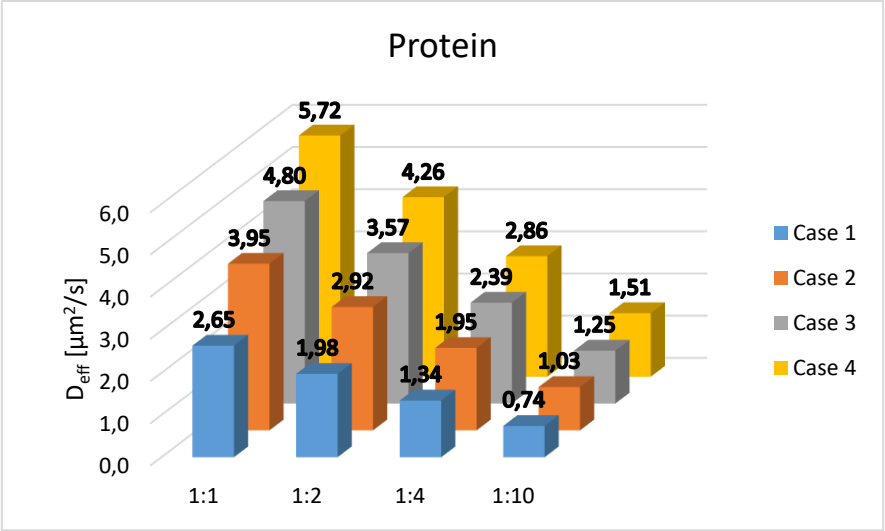

Fig. 5.14 Effective diffusion coefficients for all geometry cases for a 40 kDa protein where the free diffusion coefficient was calculated based on the Stokes-Einstein equation. The variable diffusion coefficient ratio is shown on the x-axis where the left-most is the original (1:1) without multi-scale implementation.

As the results are scaled by the free diffusion coefficient, we can see a higher effective coefficient for the protein than for dextran. Although the molecular weight of the protein and dextran may be the same, the configuration is vastly different for a polysaccharide compared to the globular structure of an enzyme. As expected, when the number and size of pits are increased, the coefficient increases, as seen from Case 1 to Case 4. As the ratio between the diffusion coefficients increases, the effective diffusivity decreases, as expected. The difference between the cases also becomes smaller. Recall that the diffusivity ratio for native wood is 1:25.

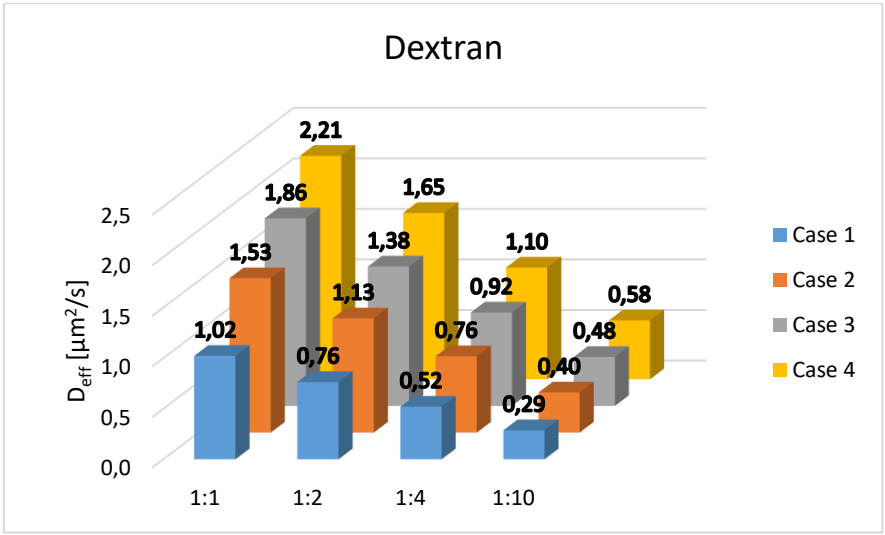

Fig. 5.15 Effective diffusion coefficients for all geometry cases for a 40 kDa dextran where the free diffusion coefficient was determined using FRAP. The variable diffusion coefficient ratio is shown on the x-axis where the left-most is the original (1:1) without multi-scale implementation.

Measurements performed with the 40 kDa dextran probe yielded diffusion coefficients in the range of 7 µm^2/s over a single earlywood tracheid. The study by Fukuyama and Hiroyuki (1986) has reported diffusion coefficients for polyethylene glycols (PEG) of 1.5 kDa of 0.7 µm^2/s. The results in Fig. 5.15 are in the range of both FRAP results presented in this work and the study of PEG by Fukuyama and Hiroyuki (1986). Important to note, however, is the scale on which

both the experiments and the simulations were performed at. As a scale increases, so does the tortuous path throughout a structure. This is especially true for the results by Fukuyama and Hiroyuki (1986) where the samples used were at the centimeter scale. On the other hand, the FRAP measurements in the present work were performed over a single tracheid, yielding the shortest path possible. An examination of the flux field in the simulations in Fig. 5.16 and Fig. 5.17, reveals the general path through the structure.

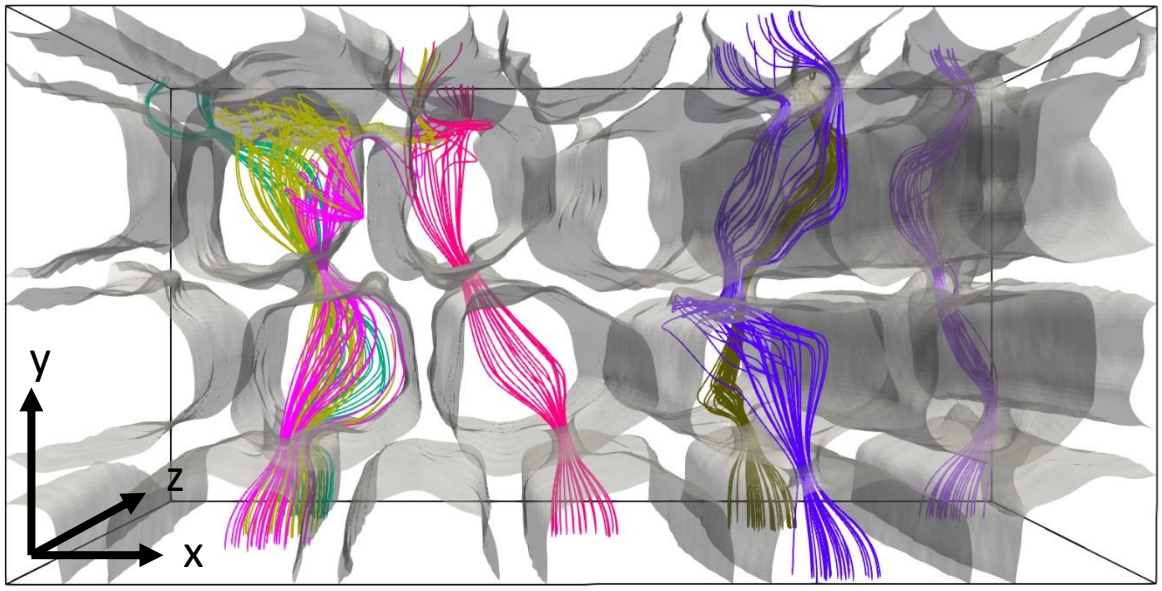

Fig. 5.16 The simulation box surrounding the surface in Case 1 with streamlines, generated from a point source, following the flux field. The radial and tangential directions are y and x, respectively, and z is longitudinal. The color of the streamlines indicates different pathways from tracheid to tracheid through the bordered pits.

An increase in the number of pits increases the number of pathways a diffusing species traverse through a structure, as seen in Case 4 in Fig. 5.17. It is important to accurately portray the connections between tracheids to obtain a correct view of mass transport in the wood microstructure. Even though the number of pits significantly increased between the case geometries, the change in effective diffusion coefficient was small by a factor of 2. This change becomes even smaller when a larger resistance is put on the pits with variable diffusion coefficients. To accurately portray the actual resistance of an undisturbed pit, an even higher ratio of close to 1:25 should be used. However, such a large difference was difficult to account for due to stability issues in the simulation.

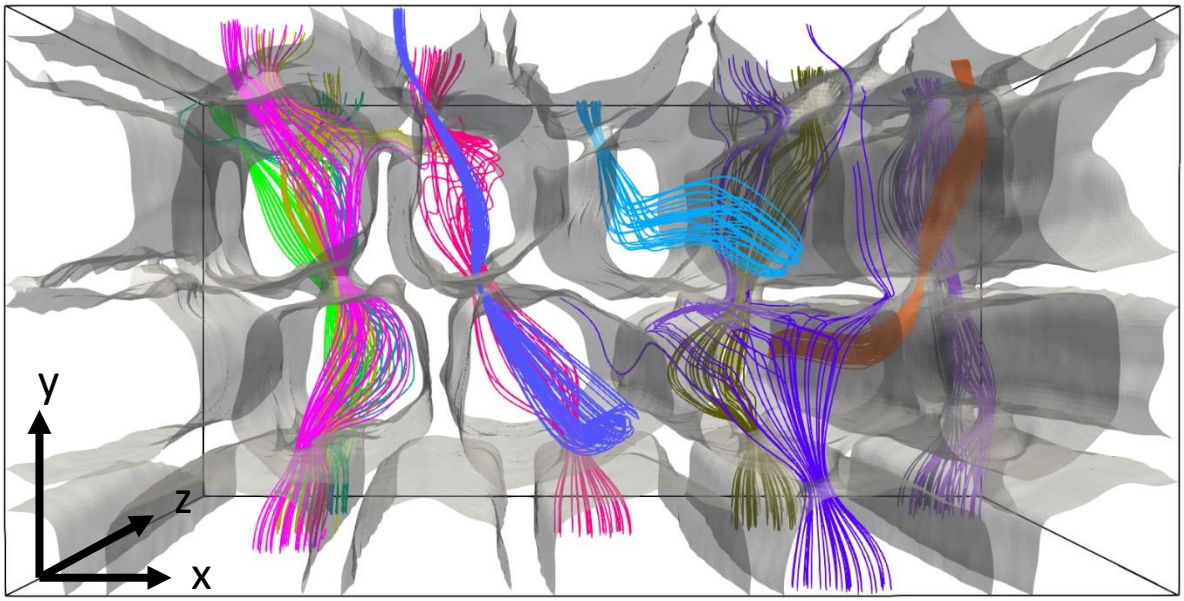

Fig. 5.17 The simulation box surrounding the surface from Case 4 with streamlines, generated from a point source, following the flux field. The radial and tangential directions are y and x, respectively, and z is longitudinal. The color of the streamlines indicates different pathways from tracheid to tracheid through the bordered pits.

6 Concluding remarks

Understanding the diffusion of large molecules is important within a materials biorefinery framework in which wood constituents of hemicellulose, cellulose, and lignin are separated into pure fractions that contain as high a molecular weight as possible. This was investigated through both experiments and mathematical modeling.

Fluorescent Recovery after Photobleaching was found to be a viable method to measure relative differences in diffusion in wood samples prepared with steam explosion. Pretreatment with steam explosion was found to have a greater effect on diffusion in the lumen network for probes of a smaller size, while larger probes showed similar resistance to diffusion in both samples. Steam explosion is able to disintegrate wood structure through collisions with chips and vessel walls, and, for this reason, the effect of this disintegration was measured at local positions to assess the increase in diffusivity in these regions at the micrometer scale.

The individual resistance of structural features of the bordered pit to diffusion was investigated. Contrary to what has been found for pressure-driven flow in which the margo and torus contribute to a major part of flow resistance, it was found that the borders totally dominate the mass transfer resistance for diffusion. Simulations of an open pit structure, which mimics steam explosion, significantly enhanced mass transfer.

Simulations of diffusion were performed at the microscale on wood pretreated with steam explosion. The structure was reconstructed based on X-ray tomography images with a resolution down to 1 micrometer. Information gathered from the simulations gave insight into the connection between structure and diffusion path, and the simulation results can easily be scaled to find the effective diffusion coefficient for a specific solute based on the free diffusion coefficient. It was found that transversal diffusion rates increase due to the pretreatment. The increase in these diffusion rates varied locally, depending on the degree of disintegration, and the local volume investigated.

One of the main issues in resolving the microscale in wood is the small features down to the sub-micrometer scale of a bordered pit. It is not computationally feasible to resolve these scales in detail. To overcome this, a multi-scale model was presented that incorporated the effective diffusion coefficient for a single pit. The effect of pretreatment on different scales was investigated by adjusting this local diffusion coefficient for bordered pits in the microstructure of wood. The methodology can be used to incorporate diffusion coefficients in different parts of the wood structure, such as latewood and cell wall, and tie scales together for a better overall

understanding of the interaction of structure and mass transport properties with regards to the pretreatment of wood.

7 References

Agbor VB, Cicek N, Sparling R, et al (2011) Biomass pretreatment: fundamentals toward application. Biotechnol Adv 29:675–85. doi: 10.1016/j.biotechadv.2011.05.005

Alvira P, Tomás-Pejó E, Ballesteros M, Negro MJ (2010) Pretreatment technologies for an efficient bioethanol production process based on enzymatic hydrolysis: A review. Bioresour Technol 101:4851–4861. doi: 10.1016/j.biortech.2009.11.093

Arrio-Dupont M, Cribier S, Foucault G, et al (1996) Diffusion of fluorescently labeled macromolecules in cultured muscle cells. Biophys J 70:2327–2332. doi: 10.1016/S0006-3495(96)79798-9

Axelrod D, Koppel DE, Schlessinger J, et al (1976) Mobility measurement by analysis of fluorescence photobleaching recovery kinetics. Biophys J 16:1055–1069. doi: 10.1016/0002-9610(76)90409-8

Azhar S, Wang Y, Lawoko M, et al (2011) Extraction of polymers from enzyme-treated softwood. BioResources 6:4606–4614

Behr EA, Briggs DR, Kaufert FH (1952) Diffusion of dissolved materials through wood. J Phys Chem 57:476–480

Bernsdorf J (2008) Simulation of complex flows and multi-physics with the Lattice-Boltzmann method. Dissertation, University of Amsterdam

Bhatnagar PL, Gross EP, Krook M (1954) A Model for Collision Processes in Gases. I. Small Amplitude Processes in Charged and Neutral One-Component Systems. Phys Rev 94:511–525

Bird RB, Stewart WE, Lightfoot EN (2007) Transport Phenomena, Rev. 2. Ed. Wiley, New York

Boving TB, Grathwohl P (2001) Tracer diffusion coefficients in sedimentary rocks: Correlation to porosity and hydraulic conductivity. J Contam Hydrol 53:85–100. doi: 10.1016/S0169-7722(01)00138-3

Brändström J (2001) Micro- and ultrastructural aspects of norway spruce tracheids: A review. IAWA J 22:333–353. doi: 10.1163/22941932-90000381

Brändström J (2002) Morphology of Norway Spruce Tracheids with Emphasis on Cell Wall Organisation. Swedish University of Agricultural sciences

Burr HK, Stamm AJ (1947) Diffusion in wood. J Phys Colloid Chem 51:240–261. doi: 10.1021/j150451a019

Cady LC, Williams JW (1934) Molecular diffusion into wood. J Phys Chem 39:87–102. doi: 10.1021/j150361a007

Cherubini F, Jungmeier G, Wellisch M, et al (2009) Toward a common classification approach for biorefinery systems. Biofuels, Bioprod Biorefining 6:534–546. doi: 10.1002/bbb.172

Christensen, G. N (1951a) Diffusion in Wood II. The Temperature Coefficient of Diffusion through Wood

Christensen, G. N (1951b) Diffusion in Wood III. Ion selection and its effect on the diffusion of electrolytes. Aust Jour Appl Sci 2:440–453

Crank J (1979) The Mathematics of Diffusion, Paperback. Clarendon Press, Oxford

Cussler EL (2009) Diffusion, Mass Transfer in Fluid Systems, 3rd ed. Cambridge University Press, Cambridge

Cuyvers S, Hendrix J, Dornez E, et al (2011) Both Substrate Hydrolysis and Secondary Substrate Binding Determine Xylanase Mobility as Assessed by FRAP. J Biol Chem 115:4810–4817

Deschout H, Raemdonck K, Demeester J, et al (2014) FRAP in pharmaceutical research: Practical guidelines and applications in drug delivery. Pharm Res 31:255–270. doi: 10.1007/s11095-013-1146-9

Doube M, Klosowski MM, Arganda-Carreras I, et al (2010) BoneJ: Free and extensible bone image analysis in ImageJ. Bone 47:1076–1079. doi: 10.1016/j.bone.2010.08.023

Einstein A (1905) Motion of suspended particles in stationary liquids required from the molecular kinetic theory of heat. Ann Phys 17:549–560. doi: 10.1002/pmic.2009.00450

Erickson HP (2009) Size and shape of protein molecules at the nanometer level determined by sedimentation, gel filtration, and electron microscopy. Biol Proced Online 11:32–51. doi: 10.1007/s12575-009-9008-x

Eshghinejadfard A, Daróczy L, Janiga G, Thévenin D (2016) Calculation of the permeability in porous media using the lattice Boltzmann method. Int J Heat Fluid Flow 1329:93–103. doi: 10.1016/j.ijheatfluidflow.2016.05.010

Fick A (1855) Ueber Diffusion. Ann Phys 170:59–86. doi: 10.1002/andp.18551700105

Fukuyama M, Hiroyuki U (1986) Diffusion of Nonelectrolytes through Wood Saturated with Water III. Diffusion rates of polyethylene glycols. JAPAN WOOD RES SOC 32:147–154

Fukuyama M, Hiroyuki U (1980) Diffusion of Nonelectrolytes through Wood Saturated with Water I. Measurement of the diffusion rates by highly sensitive differential refractometer. JAPAN WOOD RES SOC 26:587–594

Gebäck T, Heintz A (2014) A Lattice Boltzmann Method for the Advection-Diffusion Equation with Neumann Boundary Conditions. Commun Comput Phys 15:487–505. doi: 10.4208/cicp.161112.230713a

Gebäck T, Marucci M, Boissier C, et al (2015) Investigation of the Effect of the Tortuous Pore Structure on Water Diffusion through a Polymer Film Using Lattice Boltzmann Simulations. J Phys Chem B 119:5220–5227. doi: 10.1021/acs.jpcb.5b01953

Ginzburg I (2005) Equilibrium-type and link-type lattice Boltzmann models for generic

advection and anisotropic-dispersion equation. Adv Water Resour 28:1171–1195. doi: 10.1016/j.advwatres.2005.03.004

Gomes FJB, Santos F a, Colodette JL, et al (2014) Literature Review on Biorefinery Processes Integrated to the Pulp Industry. Nat Resour 5:419–432. doi: 10.4236/nr.2014.59039

Guo P, Guan Y, Liu G, et al (2016) Modeling of gas transport with electrochemical reaction in nickel-yttria-stabilized zirconia anode during thermal cycling by Lattice Boltzmann method. J Power Sources 327:127–134. doi: 10.1016/j.jpowsour.2016.07.058

Hacke UG, Sperry JS, Pitterman J (2004) Analysis of circular bordered pit function II. Gymnosperm tracheids with torus-margo pit membranes. Am J Bot 91:386–400

Hartler N (1962) Penetration and diffusion in sulfate cooking. Pap ja Puu 44:365–374

Hasunuma T, Okazaki F, Okai N, et al (2013) A review of enzymes and microbes for lignocellulosic biorefinery and the possibility of their application to consolidated bioprocessing technology. Bioresour Technol 135:513–522. doi: 10.1016/j.biortech.2012.10.047

Havimo M, Rikala J, Sirviö J, Sipi M (2008) Distributions of tracheid cross-sectional dimensions in different parts of Norway spruce stems. Silva Fenn 42:89–99

Jacobson AJ, Smith GD, Yang R, Banerjee S (2006) Diffusion of sulfide into Southern pine (Pinus taeda L.) and sweetgum (Liquidambar styraciflua L.) particles and chips. Holzforschung 60:498–502. doi: 10.1515/HF.2006.082

Jedvert K, Saltberg A, Lindström ME, Theliander H (2012a) Mild steam explosion and chemical pre-treatment of norway spruce. BioResources 7:2051–2074

Jedvert K, Wang Y, Saltberg A, et al (2012b) Mild steam explosion : A way to activate wood for enzymatic treatment, chemical pulping and biorefinery processes. Nord Pulp Pap Res J 27:828–835. doi: 10.3183/NPPRJ-2012-27-05-p828-835

Jonasson JK, Loren N, Olofsson P, et al (2008) A pixel-based likelihood framework for analysis of fluorescence recovery after photobleaching data. J Microsc 232:260–269. doi: 10.1111/j.1365-2818.2008.02097.x

Kang M, Day CA, Drake K, et al (2009) A generalization of theory for two-dimensional fluorescence recovery after photobleaching applicable to confocal laser scanning microscopes. Biophys J 97:1501–1511. doi: 10.1016/j.bpj.2009.06.017

Kapitza HG, McGregor G, Jacobson K a (1985) Direct measurement of lateral transport in membranes by using time-resolved spatial photometry. Proc Natl Acad Sci U S A 82:4122–4126. doi: 10.1073/pnas.82.12.4122

Kazi KMF, Gauvin H, Jollez P, Chornet E (1996) A diffusion model for the impregnation of lignocellulosic materials. Tappi 80:209–219

Kerr AJ, Goring DAI (1975) Ultrastructural arrangement of the wood cell wall. Cellul Chem Technol 9:563–573

Kolavali R, Theliander H (2013) Determination of the diffusion of monovalent cations into wood under isothermal conditions based on LiCl impregnation of Norway spruce. Holzforschung 67:559–565. doi: 10.1515/hf-2012-0182

Liu S, Lu H, Hu R, et al (2012) A sustainable woody biomass biorefinery. Biotechnol Adv

30:785–810. doi: 10.1016/j.biotechadv.2012.01.013

Liu Z, Wu H (2016) Pore-scale study on flow and heat transfer in 3D reconstructed porous media using micro-tomography images. Appl Therm Eng 100:602–610. doi: 10.1016/j.applthermaleng.2016.02.057

Lopez-Sanchez P, Schuster E, Wang D, et al (2015) Diffusion of macromolecules in self-assembled cellulose/hemicellulose hydrogels. Soft Matter 11:4002–4010. doi: 10.1039/C5SM00103J

Lorén N, Hagman J, Jonasson JK, et al (2015) Fluorescence recovery after photobleaching in material and life sciences: putting theory into practice. Q Rev Biophys 48:323–387. doi: 10.1017/S0033583515000013

Ma Q, Zhao Z, Xu M, et al (2016) The pit membrane changes of micro-explosion-pretreated poplar. Wood Sci Technol 50:1089–1099. doi: 10.1007/s00226-016-0841-1

Maire E (2012) X-Ray Tomography Applied to the Characterization of Highly Porous Materials. Annu Rev Mater Res 42:163–178. doi: 10.1146/annurev-matsci-070511-155106

Mattsson T, Azhar S, Eriksson S, et al (2017) The Development of a Wood-based Materials-biorefinery. BioResources 12:9152–9182. doi: 10.15376/biores.7.4.4501-4516

Meyer F (1994) Topographic distance and watershed lines. Signal Processing 38:113–125. doi: 10.1016/0165-1684(94)90060-4

Mohamad AA (2011) Lattice Boltzmann Method. Springer London, London

Muzamal M, Bååth Arnling J, Olsson L, Rasmuson A (2016) Contribution of Structural Modification to Enhanced Enzymatic Hydrolysis and 3-D Structural Analysis of Steam-Exploded Wood using X-Ray Tomography. BioResources 11:8509–8521

Muzamal M, Gamstedt EK, Rasmuson A (2014) Modeling wood fiber deformation caused by vapor expansion during steam explosion of wood. Wood Sci Technol 48:353–372. doi: 10.1007/s00226-013-0613-0

Muzamal M, Jedvert K, Theliander H, Rasmuson A (2015) Structural changes in spruce wood during different steps of steam explosion pretreatment. Holzforschung 69:61–66. doi: 10.1515/hf-2013-0234

Muzamal M, Rasmuson A (2017) Dynamic simulation of disintegration of wood chips caused by impact and collisions during the steam explosion pretreatment. Wood Sci Technol 51:115–131. doi: 10.1007/s00226-016-0840-2

Narayanamurti D, Kumar VB (1953) Diffusion of organic molecules through wood. J Polym Sci 10:515–524. doi: 10.1002/pol.1953.120100602

Paës G, Chabbert B (2012) Characterization of arabinoxylan/cellulose nanocrystals gels to investigate fluorescent probes mobility in bioinspired models of plant secondary cell wall. Biomacromolecules 13:206–214. doi: 10.1021/bm201475a

Paës G, Habrant A, Ossemond J, Chabbert B (2017) Exploring accessibility of pretreated poplar cell walls by measuring dynamics of fluorescent probes. Biotechnol Biofuels 10:15. doi: 10.1186/s13068-017-0704-5

Paës G, von Schantz L, Ohlin M (2015) Bioinspired assemblies of plant cell wall polymers

unravel the affinity properties of carbohydrate-binding modules. Soft Matter 11:6586–6594. doi: 10.1039/C5SM01157D

Peixoto PDS, Bouchoux A, Huet S, et al (2015) Diffusion and partitioning of macromolecules in casein microgels: Evidence for size-dependent attractive interactions in a dense protein system. Langmuir 31:1755–1765. doi: 10.1021/la503657u

Petty JA (1973) Diffusion of non-swelling gases through dry conifer wood. Wood Sci Technol 7:297–307. doi: 10.1007/BF00351075

Petty JA (1972) The aspiration of bordered wood pits in conifer wood. Proc R Soc London 181:395–406. doi: 10.1098/rspb.1972.0057

Plötze M, Niemz P (2010) Porosity and pore size distribution of different wood types as determined by mercury intrusion porosimetry. Eur J Wood Wood Prod 649–657. doi: 10.1007/s00107-010-0504-0

Schneider C a, Rasband WS, Eliceiri KW (2012) NIH Image to ImageJ: 25 years of image analysis. Nat Methods 9:671–675. doi: 10.1038/nmeth.2089

Schulte PJ (2012) Computational fluid dynamics models of conifer bordered pits show how pit structure affects flow. New Phytol 193:721–729. doi: 10.1111/j.1469-8137.2011.03986.x

Schulte PJ, Hacke UG, Schoonmaker AL (2015) Pit membrane structure is highly variable and accounts for a major resistance to water flow through tracheid pits in stems and roots of two boreal conifer species. New Phytol 208:102–113. doi: 10.1111/nph.13437

Schuster E, Eckardt J, Hermansson A-M, et al (2014) Microstructural, mechanical and mass transport properties of isotropic and capillary alginate gels. Soft Matter 10:357–66. doi: 10.1039/c3sm52285g

Schuster E, Sott K, Ström A, et al (2016) Interplay between flow and diffusion in capillary alginate hydrogels. Soft Matter 12:3897–907. doi: 10.1039/c6sm00294c

Sellen DB (1975) Light scattering rayleigh linewidth measurements on some macromolecular solutions. J Polym Sci Polym Symp 16:561–564. doi: 10.1002/polc.5070420319

Shen L, Chen Z (2007) Critical review of the impact of tortuosity on diffusion. Chem Eng Sci 62:3748–3755. doi: 10.1016/j.ces.2007.03.041

Siau JF (1984) Transport Processes in Wood. Springer Berlin Heidelberg

Sjöström E (1993) Wood chemistry: Fundamentals and Applications, 2nd edn. Academic Press, Inc., San Diego, California

Stamm A (1946) Passage of liquids, vapors, and dissolved materials through softwoods. Tech Bull - US Dept Agric 84

Trtik P, Dual J, Keunecke D, et al (2007) 3D imaging of microstructure of spruce wood. J Struct Biol 159:46–55. doi: 10.1016/j.jsb.2007.02.003

Valli A, Koponen A, Vesala T, Timonen J (2002) Simulations of water flow through boredered pits of conifer xylem. J Statiscal Phys 107:121–142

Van den Bulcke J, Biziks V, Andersons B, et al (2013) Potential of X-ray computed tomography for 3D anatomical analysis and microdensitometrical assessment in wood research with focus on wood modification. Int Wood Prod J 4:183–190. doi:

10.1179/2042645313y.0000000046

Videcoq P, Steenkeste K, Bonnin E, Garnier C (2013) A multi-scale study of enzyme diffusion in macromolecular solutions and physical gels of pectin polysaccharides. Soft Matter 9:5110–5118. doi: 10.1039/c3sm00058c

Wadsö L (1988) BORDERED PIT DIFFUSION, Report TVBM-3034. Lund Institute of Technology, Sweden

Wang K, Jiang JX, Xu F, Sun RC (2009) Influence of steaming explosion time on the physic-chemical properties of cellulose from Lespedeza stalks (Lespedeza crytobotrya). Bioresour Technol 100:5288–5294. doi: 10.1016/j.biortech.2009.05.019

Wassén S, Bordes R, Gebäck T, et al (2014) Probe diffusion in phase-separated bicontinuous biopolymer gels. Soft Matter 10:8276–8287. doi: 10.1039/c4sm01513d

Xia M (2016) Pore-scale simulation of miscible displacement in porous media using the lattice Boltzmann method. Comput Geosci 88:30–40. doi: 10.1016/j.cageo.2015.12.014

Yang B, Wyman C (2012) Pretreatment: the key to unlocking low-cost cellulosic ethanol. Biofuels, Bioprod Biorefining 6:246–256. doi: 10.1002/bbb

Yang D, Moran-mirabal JM, Parlange J, Walker LP (2013) Investigation of the Porous Structure of Cellulosic Substrates Through Confocal Laser Scanning Microscopy. Biotechnol Bioeng 110:2836–2845. doi: 10.1002/bit.24958

Zauer M, Hempel S, Pfriem A, et al (2014) Investigations of the pore-size distribution of wood in the dry and wet state by means of mercury intrusion porosimetry. Wood Sci Technol 48:1229–1240. doi: 10.1007/s00226-014-0671-y

Zauer M, Pfriem A, Wagenführ A (2013) Toward improved understanding of the cell-wall density and porosity of wood determined by gas pycnometry. Wood Sci Technol 47:1197–1211. doi: 10.1007/s00226-013-0568-1

Zhang X, Crawford JW, Flavel RJ, Young IM (2016a) A multi-scale Lattice Boltzmann model for simulating solute transport in 3D X-ray micro-tomography images of aggregated porous materials. J Hydrol 541:1020–1029. doi: 10.1016/j.jhydrol.2016.08.013

Zhang X, Crawford JW, Young IM (2016b) A Lattice Boltzmann model for simulating water flow at pore scale in unsaturated soils. J Hydrol 538:152–160. doi: 10.1016/j.jhydrol.2016.04.013

Zhang Y, Cai L (2006) Effects of steam explosion on wood appearance and structure of sub-alpine fir. Wood Sci Technol 40:427–436. doi: 10.1007/s00226-005-0053-6

Zhou JG (2004) Lattice Boltzmann Methods for Shallow Water Flows. Springer, Berlin